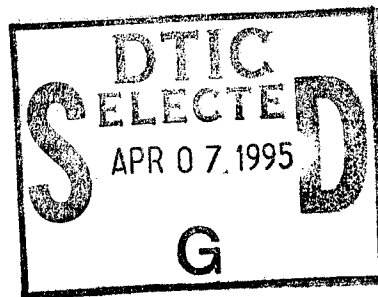


# NAVAL POSTGRADUATE SCHOOL Monterey, California



**THESIS**

**CONTROL OF FLEXIBLE  
SPACECRAFT STRUCTURES USING  
H-INFINITY WAVE ABSORBING CONTROL**

by

Ronald E. Strong

December 1994

Thesis Advisor:

Brij N. Agrawal

**Approved for public release; distribution is unlimited**

19950405 024

DTIC QUALITY INSPECTED 1

REPORT DOCUMENTATION PAGE			Form Approved OMB No. 0704	
Public reporting burden for this collection of information is estimated to average 1 hour per response, including the time for reviewing instruction, searching existing data sources, gathering and maintaining the data needed, and completing and reviewing the collection of information. Send comments regarding this burden estimate or any other aspect of this collection of information, including suggestions for reducing this burden, to Washington headquarters Services, Directorate for Information Operations and Reports, 1215 Jefferson Davis Highway, Suite 1204, Arlington, VA 22202-4302, and to the Office of Management and Budget, Paperwork Reduction Project (0704-0188) Washington DC 20503.				
1. AGENCY USE ONLY (Leave blank)		2. REPORT DATE December 1994	3. REPORT TYPE AND DATES COVERED Master's Thesis	
4. TITLE AND SUBTITLE CONTROL OF FLEXIBLE SPACECRAFT STRUCTURES USING H-INFINITY WAVE ABSORBING CONTROL			5. FUNDING NUMBERS	
6. AUTHOR(S) Strong, Ronald E.				
7. PERFORMING ORGANIZATION NAME(S) AND ADDRESS(ES) Naval Postgraduate School Monterey CA 93943-5000			8. PERFORMING ORGANIZATION REPORT NUMBER	
9. SPONSORING/MONITORING AGENCY NAME(S) AND ADDRESS(ES)			10. SPONSORING/MONITORING AGENCY REPORT NUMBER	
11. SUPPLEMENTARY NOTES The views expressed in this thesis are those of the author and do not reflect the official policy or position of the Department of Defense or the U.S. Government.				
12a. DISTRIBUTION/AVAILABILITY STATEMENT Approved for public release; distribution unlimited			12b. DISTRIBUTION CODE	
13. ABSTRACT (Maximum 200 words)  This work studies the use of a wave absorbing control law for vibration suppression of flexible spacecraft structures. A major advantage of this method is that it does not involve truncation into a finite dimensional mathematical model. A closed loop scattering matrix was derived which gives the relationship between incoming waves, outgoing waves, sensor and actuator. The control law was determined by minimizing the H-infinity norm of this matrix. The control law was applied to the Naval Postgraduate School's Flexible Spacecraft Simulator (FSS) for vibration suppression. The simulator's flexible beam was controlled using piezoceramic wafers as sensors and actuators. The H-infinity wave absorbing controller contributed significant damping to the structure, especially at the first mode of 1 Hz. Therefore, wave absorbing control and piezoceramic sensors and actuators offer a viable approach for vibration suppression of space structures.				
14. SUBJECT TERMS Smart Structure, Wave Absorbing Control, H-infinity Control, Piezoelectric			15. NUMBER OF PAGES 68	
			16. PRICE CODE	
17. SECURITY CLASSIFICATION OF REPORT  Unclassified	18. SECURITY CLASSIFICATION OF THIS PAGE  Unclassified	19. SECURITY CLASSIFICATION OF ABSTRACT  Unclassified	20. LIMITATION OF ABSTRACT  UL	



Approved for public release; distribution is unlimited

**CONTROL OF FLEXIBLE SPACECRAFT STRUCTURES  
USING H-INFINITY WAVE ABSORBING CONTROL**

by

Ronald E. Strong  
Lieutenant, United States Navy Reserve  
B.S. Mechanical Engineering, University of Utah, 1986

Submitted in partial fulfillment  
of the requirements for the degree of

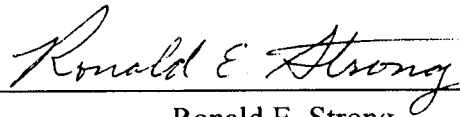
**MASTER OF SCIENCE IN ASTRONAUTICAL ENGINEERING**

from the

**NAVAL POSTGRADUATE SCHOOL**

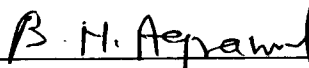
December 1994

Author:

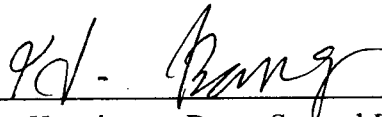


Ronald E. Strong

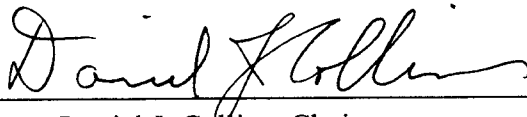
Approved by:



Brij N. Agrawal, Thesis Advisor



Hyochoong Bang, Second Reader



Daniel J. Collins, Chairman  
Department of Aeronautical/Astronautical Engineering



## ABSTRACT

This work studies the use of a wave absorbing control law for vibration suppression of flexible spacecraft structures. A major advantage of this method is that it does not involve truncation into a finite dimensional mathematical model. A closed loop scattering matrix was derived which gives the relationship between incoming waves, outgoing waves, sensor, and actuator. The control law was determined by minimizing the H-infinity norm of this matrix. The control law was applied to the Naval Postgraduate School's Flexible Spacecraft Simulator (FSS) for vibration suppression. The simulator's flexible beam was controlled using piezoelectric ceramic wafers as sensors and actuators. The H-infinity wave absorbing controller contributed significant damping to the structure, especially at the first mode of 1 Hz. Therefore, wave absorbing control and piezoceramic sensors and actuators offer a viable approach for vibration suppression of space structures.

Accession For	
NTIS CRA&I	<input checked="" type="checkbox"/>
DTIC TAB	<input type="checkbox"/>
Unannounced	<input type="checkbox"/>
Justification .....	
By .....	
Distribution /	
Availability Codes	
Dist	Avail and/or Special
A-1	

1. The first part of the document discusses the importance of maintaining accurate records of all transactions and activities. It emphasizes that proper record-keeping is essential for ensuring transparency and accountability in financial reporting.

2. The second part of the document outlines the various methods and techniques used to collect and analyze data. It highlights the need for a systematic approach to data collection and the importance of using reliable sources of information.

3. The third part of the document focuses on the analysis and interpretation of the collected data. It discusses the various statistical and analytical tools that can be used to identify trends and patterns in the data.

4. The fourth part of the document discusses the importance of communicating the results of the analysis to the relevant stakeholders. It emphasizes the need for clear and concise reporting and the importance of providing context and interpretation for the findings.

5. The fifth part of the document discusses the various challenges and limitations associated with data collection and analysis. It highlights the need for a thorough understanding of the data and the importance of being transparent about any limitations or biases that may be present.

## TABLE OF CONTENTS

I.	INTRODUCTION.....	1
A.	BACKGROUND.....	1
B.	FOCUS OF THESIS.....	1
II.	THEORETICAL ANALYSIS.....	3
A.	WAVE ABSORBING CONTROL.....	3
1.	Dynamic Model.....	3
a.	Laplace Transform Solution to Beam Equation.....	4
b.	State Space Representation.....	5
c.	State Vector in Terms of Travelling Waves.....	7
d.	Boudary Conditions.....	11
2.	Control Law.....	12
a.	System Equation in Four Block Form.....	12
b.	H-infinity Compensator Design.....	15
B.	SENSOR AND ACTUATOR.....	18
1.	Piezoelectric Material.....	18
2.	Sensor.....	19
3.	Actuator.....	20
III.	STRUCTURAL RESPONSE SIMULATION.....	23
A.	OPEN LOOP TRANSFER FUNCTION.....	23
B.	DISCRETE TRANSFER FUNCTION.....	28
C.	CLOSED LOOP SYSTEM.....	29
D.	SIMULATION RESULTS.....	29



IV.	EXPERIMENTAL ANALYSIS.....	33
A.	SET UP.....	33
B.	EXPERIMENTAL RESULTS.....	36
1.	Initial Tests.....	36
2.	Free Response of the Beam.....	37
3.	Initial Condition Response with Active Control.....	39
4.	Forced Response.....	41
V.	CONCLUSIONS.....	43
	APPENDIX A.....	45
	APPENDIX B.....	51
	APPENDIX C.....	53
	LIST OF REFERENCES.....	55
	INITIAL DISTRIBUTION LIST.....	57



## ACKNOWLEDGEMENTS

The author would like to express his appreciation to Dr Hyochoong Bang who contributed many hours of tutoring. His guidance in the use of the AC-100<sup>TM</sup> real time control system and the Flexible Spacecraft Simulator was very helpful and his insights in the areas of wave absorbing and robust control theory were invaluable in the completion of this project. An equal amount of thanks goes to Dr. Brij N. Agrawal for providing the resources used with this project and for guiding the project. His course in Flexible Spacecraft Structures was very helpful in understanding the dynamics involved in this project. His patience and encouragement during difficult times were greatly appreciated.

## I. INTRODUCTION

### A. BACKGROUND

Recent trends in spacecraft design have led to larger and more flexible structures. Large structures such as Space Station Freedom pose interesting new problems in structural dynamics and control. In addition, modern sensor equipment has become more and more accurate, making it highly sensitive to structural vibration. For example, an antenna or optical sensor, requiring a high degree of pointing accuracy may be mounted on a flexible structure connected to the spacecraft bus. The antenna will be subjected to vibration from the spacecraft bus due to slew maneuvers, momentum wheel vibration, and thruster firing. Passive vibration isolation can absorb some of the energy. However, modern payloads have led to a requirement for active vibration control and isolation.

There have been two major approaches to vibration control of flexible structures. The first, and more conventional approach, is based on modal control of the structure such as described by Newman [Ref. 1]. This approach usually suffers from modeling errors and state estimation. The use of modal model based control laws has been an area of intense research during the last decade. The second approach describes the structural response in terms of an elastic disturbance which travels through the structure. [Ref. 2] In this approach, compensators are designed to reduce the effects of incoming waves on outgoing waves. The advantages of the wave absorbing approach are:

- Relatively simple to implement
- Broadband control
- Does not require finite element analysis or modal model

## **B. FOCUS OF THESIS**

This thesis concentrates on three areas. First, a wave absorbing controller will be derived using an H-infinity approach similar to one used by Matsuda and Fuji [Ref. 3]. Second, the control law will be simulated using a finite element model of the beam to be studied. The transfer function of the open loop system will be found using modal truncation, then the loop will be closed with the H infinity controller. Last, the control law will be implemented on the Naval Postgraduate School's Flexible Spacecraft Simulator (FSS). The control law will be applied by a real time control system using Matrix<sub>x</sub><sup>TM</sup>, System Build<sup>TM</sup>, and AC-100 by Integrated Systems Incorporated (ISI). The results of the experiment will be compared the analytical computer simulation.

## II. THEORETICAL ANALYSIS

### A. WAVE ABSORBING CONTROL

This thesis approaches active control of the Flexible Spacecraft Simulator (FSS) using a wave absorbing control theory. The response of the beam is viewed as a travelling elastic disturbance due to a locally applied force. This approach has been developed by a number of sources such as von Flotow and Shafer [Ref. 4], MacMartin and Hall [Ref. 5], Matsuda and Fuji [Ref. 3] and Fuji et al. [Ref. 6].

#### 1. Dynamic Model

The FSS setup is shown in Figure 1. The base of the flexible beam is fixed to the center body with the other end of the beam free. Using the Euler-Bernoulli beam theory the dynamics of a flexible beam are given by the following partial differential equation:

$$EI \frac{\partial^4 w}{\partial x^4} + \rho A \frac{\partial^2 w}{\partial t^2} = 0 \quad (2.1)$$

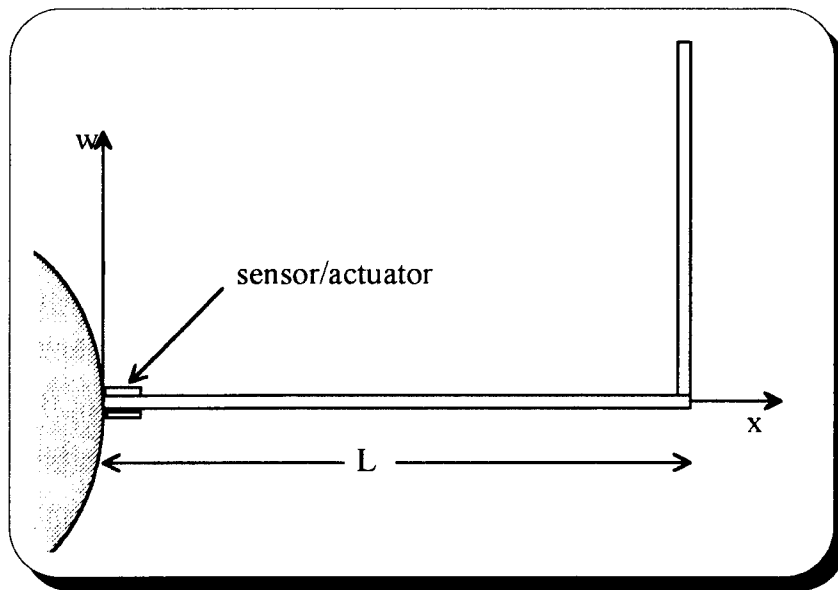


Figure 1. FSS Beam Model

The boundary conditions are :

$$\text{Clamped end:} \quad w(0, t) = 0, \quad \dot{w}(0, t) = 0 \quad (2.2)$$

$$\text{Actuator moment:} \quad EI \frac{\partial^2 w}{\partial x^2}(0, t) = M_c \quad (2.3)$$

where  $w(x, t)$  is the lateral displacement,  $M_c$  is the bending moment,  $EI$  is the bending rigidity, and  $\rho A$  is the mass per unit length. The moment and shear force at the free end are zero, but will not be necessary for the derivation. As can be seen in equation (2.3), the control forces can be accounted for via the boundary conditions, which allows the force term on the right hand side of equation (2.1) to be taken as zero.

**a. Laplace Transform Solution to Beam Equation**

The partial differential equation (2.1) can be analyzed using the Laplace transform. The initial conditions,  $w(x, 0)$  and  $\dot{w}(x, 0)$  are assumed to be zero. The nonzero values of  $w(x, 0)$  and  $\dot{w}(x, 0)$  obviously do not make a difference in the final result.

$$L[w(x, t)] = W(x, s) = \int_0^\infty w(x, t)e^{-st} dt \quad (2.4)$$

$$L\left[\frac{\partial^2 w}{\partial t^2}\right] = s^2 W(x, s) \quad (2.5)$$

$$L\left[\frac{\partial^4 w}{\partial x^4}\right] = \int_0^\infty \frac{\partial^4 w}{\partial x^4} e^{-st} dt = \frac{d^4}{dx^4} W(x, s) \quad (2.6)$$

The fourth order partial derivative becomes an ordinary derivative since time is "frozen" in the s domain. This reduces the Euler-Bernoulli beam equation to:

$$a^2 \frac{d^4 W(x, s)}{dx^4} + s^2 W(x, s) = 0 \quad (2.7)$$

where

$$a^2 = \frac{EI}{\rho A} \quad (2.8)$$

**b. State Space Representation**

The analysis of equation (2.7) can be simplified by using state space methods. A state vector containing the cross sectional properties of the beam is introduced.

$$Y = \begin{Bmatrix} y_1 \\ y_2 \\ y_3 \\ y_4 \end{Bmatrix} = \begin{Bmatrix} \dot{w} \\ \dot{\theta} \\ \frac{a}{EI}M \\ \frac{a}{EI}Q \end{Bmatrix} \quad (2.9)$$

where,

$$\begin{aligned} \dot{w} = s w & \text{ is the lateral velocity} \\ \dot{\theta} = s \frac{dw}{dx} & \text{ is the angular velocity} \\ M = EI \frac{d^2 w}{dx^2} & \text{ is the internal bending moment} \\ Q = EI \frac{d^3 w}{dx^3} & \text{ is the internal shear moment} \end{aligned}$$

The state vector (2.9) can be used to transform equation (2.7) to a set of first order state equations in terms of  $x$  in the form:

$$\frac{dY}{dx} = AY \quad (2.10)$$

Let us introduce  $p = \frac{s}{a}$  and proceed as follows.

$$\frac{dy_1}{dx} = \frac{d\dot{w}}{dx} = \dot{\theta} = y_2 \quad (2.11)$$

$$\frac{dy_2}{dx} = s \frac{d\theta}{dx} = s \frac{d^2 w}{dx^2} = s \frac{M}{EI} = \frac{s}{a} y_3 = p y_3 \quad (2.12)$$



$$\frac{dy_3}{dx} = \frac{a}{EI} \frac{dM}{dx} = \frac{a}{EI} Q = y_4 \quad (2.13)$$

$$\frac{dy_4}{dx} = \frac{a}{EI} \frac{dQ}{dx} = \frac{a}{EI} (EI \frac{d^4 w}{dx^4}) = a \frac{d^4 w}{dx^4} \quad (2.14)$$

Using the dynamic system equation (2.7) we can determine  $\frac{dy_4}{dx}$  as

$$\frac{d^4 w}{dx^4} = -\frac{s^2}{a^2} w \quad (2.15)$$

Therefore

$$\frac{dy_4}{dx} = -psw = -p\dot{w} = -py_1 \quad (2.16)$$

This leads to the state equation:

$$\frac{dY}{dx} = \begin{bmatrix} 0 & 1 & 0 & 0 \\ 0 & 0 & p & 0 \\ 0 & 0 & 0 & 1 \\ -p & 0 & 0 & 0 \end{bmatrix} Y = AY \quad (2.17)$$

The solution of the ordinary differential equation shown above is given by

$$\begin{aligned} Y(x) &= e^{Ax} Y(0) \\ &= U e^{\Lambda x} U^{-1} Y(0) \end{aligned} \quad (2.18)$$

where  $\Lambda$  is found by similarity transformation of  $A$ . This can be done by solving the following eigenvalue problem.

$$U\Lambda = AU \quad (2.19)$$

$$\Lambda = \sqrt{\frac{p}{2}} \begin{bmatrix} \lambda_1 & 0 & 0 & 0 \\ 0 & \lambda_2 & 0 & 0 \\ 0 & 0 & \lambda_3 & 0 \\ 0 & 0 & 0 & \lambda_4 \end{bmatrix} \quad (2.20)$$

$$U = \begin{bmatrix} 1 & 1 & 1 & 1 \\ \lambda_1 & \lambda_2 & \lambda_3 & \lambda_4 \\ \frac{\lambda_1^2}{p} & \frac{\lambda_2^2}{p} & \frac{\lambda_3^2}{p} & \frac{\lambda_4^2}{p} \\ \frac{\lambda_1^3}{p} & \frac{\lambda_2^3}{p} & \frac{\lambda_3^3}{p} & \frac{\lambda_4^3}{p} \end{bmatrix} \quad (2.21)$$

where the eigenvalues are

$$\lambda = \begin{Bmatrix} 1 + i \\ 1 - i \\ -1 + i \\ -1 - i \end{Bmatrix} \quad (2.22)$$

As can be seen from equations (2.18-22), the solution yields imaginary solutions. A more useful solution can be transforming the matrix A or its diagonal transformation to real Jordan canonical form. [Ref. 3] As discussed in the next section this will also yield a state vector in terms of travelling waves instead of cross sectional variables.

*c. State Vector in Terms of Travelling Waves*

The state vector Y from the previous section is defined in terms of the cross sectional variables of the beam. As stated at the beginning of this chapter, we desire to study the disturbances in the beam in terms of travelling waves. The matrix  $\Lambda$  can be transformed to real Jordan canonical form by the matrix K. [Ref. 7, pp 144,145]

$$K = \begin{bmatrix} \frac{1}{2} & -\frac{i}{2} & 0 & 0 \\ \frac{1}{2} & \frac{i}{2} & 0 & 0 \\ 0 & 0 & \frac{1}{2} & -\frac{i}{2} \\ 0 & 0 & \frac{1}{2} & \frac{i}{2} \end{bmatrix} \quad (2.23)$$

The new matrix  $\bar{A}$  can then be formed by the similarity transformation

$$\bar{A} = (K^{-1}U^{-1})A(UK) = P^{-1}AP \quad (2.24)$$

where

$$P = UK = \frac{1}{2} \begin{bmatrix} \sqrt{2}p & 0 & \sqrt{2}p & 0 \\ p^{\frac{2}{3}} & p^{\frac{2}{3}} & -p^{\frac{2}{3}} & p^{\frac{2}{3}} \\ 0 & \sqrt{2}p & 0 & -\sqrt{2}p \\ -p^{\frac{2}{3}} & p^{\frac{2}{3}} & p^{\frac{2}{3}} & p^{\frac{2}{3}} \end{bmatrix} \quad (2.25)$$

Using this transformation the state vector can be changed to

$$Y = PV \quad (2.26)$$

where the new state vector  $V$  contains the amplitudes of the travelling wave modes.

$$V = \begin{Bmatrix} a_1 \\ a_2 \\ b_1 \\ b_2 \end{Bmatrix} \quad (2.27)$$

This notation is similar to that used in literature used in microwave circuits. [Ref. 4, pg. 674] At any point along the beam the motion can be described by four modes, two incoming and two outgoing waves as shown in Figure 2.

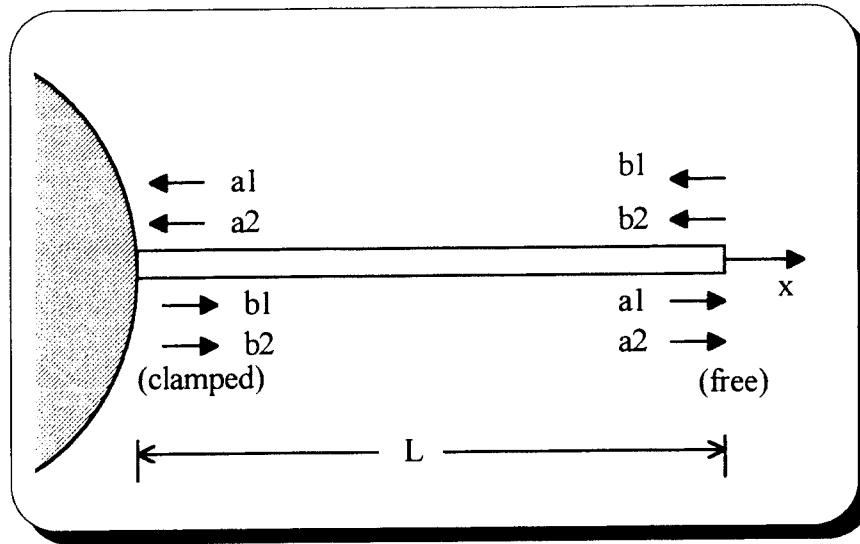


Figure 2. Travelling Wave Modes

The new state vector varies with position along the beam according to the new state equation

$$\frac{dV}{dx} = \bar{A}V = \sqrt{\frac{p}{2}} \begin{bmatrix} 1 & 1 & 0 & 0 \\ 1 & 1 & 0 & 0 \\ 0 & 0 & -1 & 1 \\ 0 & 0 & -1 & -1 \end{bmatrix} V \quad (2.28)$$

Equation (2.28) has a solution of the form

$$V(x) = e^{Ax} V(0) \quad (2.29)$$

The matrix  $e^{Ax}$  can be represented by

$$e^{Ax} = \begin{bmatrix} e^{\bar{A}_1 x} & 0 \\ 0 & e^{\bar{A}_2 x} \end{bmatrix} \quad (2.30)$$

where  $\bar{A}_1$  and  $\bar{A}_2$  are the block diagonals of  $\bar{A}$ .

Next the inverse Laplace transform (with respect to  $x$ )

$$e^{Ax} = L^{-1}[(sI - A)^{-1}] \quad (2.31)$$

is used to find the exponentials along the diagonal of equation (2.30). Let  $c = \sqrt{\frac{p}{2}}$ , then

$$(sI - A_1) = \begin{bmatrix} s - c & -c \\ c & s - c \end{bmatrix} \quad (2.32)$$

$$(sI - A_1)^{-1} = \frac{1}{(s-c)^2 + c^2} \begin{bmatrix} s - c & c \\ -c & s - c \end{bmatrix} \quad (2.33)$$

By taking the inverse Laplace transform using equation (2.31) the first diagonal element of equation (2.30) is found.

$$e^{A_1 x} = \begin{bmatrix} e^{cx} \cos cx & e^{cx} \sin cx \\ -e^{cx} \sin cx & e^{cx} \cos cx \end{bmatrix} \quad (2.34)$$

The second diagonal element can be found in a similar fashion leading to the solution

$$V(x) = \begin{bmatrix} e^{cx} \cos cx & e^{cx} \sin cx & 0 & 0 \\ -e^{cx} \sin cx & e^{cx} \cos cx & 0 & 0 \\ 0 & 0 & e^{-cx} \cos cx & e^{-cx} \sin cx \\ 0 & 0 & -e^{-cx} \sin cx & e^{-cx} \cos cx \end{bmatrix} V(0) \quad (2.35)$$

To determine the wave amplitudes for the pinned and free end of the beam in Figure 2, the solution is determined for  $x = L$ . This leads to the same solution as determined by Matsuda and Fuji. [Ref. 3]

$$\begin{Bmatrix} a_1 \\ a_2 \\ b_1 \\ b_2 \end{Bmatrix} (L) = \begin{bmatrix} e^{cx} \cos cx & e^{cx} \sin cx & 0 & 0 \\ -e^{cx} \sin cx & e^{cx} \cos cx & 0 & 0 \\ 0 & 0 & e^{-cx} \cos cx & e^{-cx} \sin cx \\ 0 & 0 & -e^{-cx} \sin cx & e^{-cx} \cos cx \end{bmatrix} \begin{Bmatrix} a_1 \\ a_2 \\ b_1 \\ b_2 \end{Bmatrix} (0) \quad (2.36)$$

**d. Boundary Conditions**

The boundary conditions are given by equations (2.2) and (2.3). The boundary conditions can be transformed to the new coordinates by equation (2.25).

$$\begin{bmatrix} 1 & 0 & 0 & 0 \\ 0 & 0 & \frac{EI}{a} & 0 \end{bmatrix} \begin{Bmatrix} \dot{w} \\ \dot{\theta} \\ \frac{a}{EI} M \\ \frac{a}{EI} Q \end{Bmatrix} = \begin{Bmatrix} 0 \\ M_c \end{Bmatrix} \quad (2.37)$$

which can be rewritten as

$$\begin{bmatrix} 1 & 0 & 0 & 0 \\ 0 & 0 & \frac{EI}{a} & 0 \end{bmatrix} \left(\frac{1}{2}\right) \begin{bmatrix} \sqrt{2}p & 0 & \sqrt{2}p & 0 \\ p^{\frac{2}{3}} & p^{\frac{2}{3}} & -p^{\frac{2}{3}} & p^{\frac{2}{3}} \\ 0 & \sqrt{2}p & 0 & -\sqrt{2}p \\ -p^{\frac{2}{3}} & p^{\frac{2}{3}} & p^{\frac{2}{3}} & p^{\frac{2}{3}} \end{bmatrix} \begin{Bmatrix} a_1 \\ a_2 \\ b_1 \\ b_2 \end{Bmatrix} = \begin{Bmatrix} 0 \\ M_c \end{Bmatrix} \quad (2.38)$$

or

$$\begin{bmatrix} \frac{1}{2}\sqrt{2}p & 0 & \frac{1}{2}\sqrt{2}p & 0 \\ 0 & \frac{EI}{2a}\sqrt{2}p & 0 & -\frac{EI}{2a}\sqrt{2}p \end{bmatrix} \begin{Bmatrix} a_1 \\ a_2 \\ b_1 \\ b_2 \end{Bmatrix} = \begin{Bmatrix} 0 \\ M_c \end{Bmatrix} \quad (2.39)$$

This equation can be solved for the outgoing wave amplitudes  $[b_1, b_2]$  as a function of the incoming wave modes  $[a_1, a_2]$  and the control moment  $M_c$ .

$$\begin{Bmatrix} b_1 \\ b_2 \end{Bmatrix} = \begin{bmatrix} -1 & 0 \\ 0 & 1 \end{bmatrix} \begin{Bmatrix} a_1 \\ a_2 \end{Bmatrix} + \begin{Bmatrix} 0 \\ -\frac{\sqrt{2}}{p} \end{Bmatrix} \frac{a}{EI} M_c \quad (2.40)$$

## 2. Control Law

### a. System Equation in Four Block Form

The wave equations derived in Section 1 can be written as a standard four block form in robust control theory. The equations are as follows.

$$b = Sa + Bu \quad (2.41)$$

$$y = Ta + Gu \quad (2.42)$$

where the matrix  $S$ , which in this special case is called the scattering matrix contains the reflection coefficients. The standard four block form is written as

$$\begin{Bmatrix} b \\ y \end{Bmatrix} = \begin{bmatrix} S & B \\ T & G \end{bmatrix} \begin{Bmatrix} a \\ u \end{Bmatrix} \quad (2.43)$$

The block diagram for this system is shown in Figure 3.

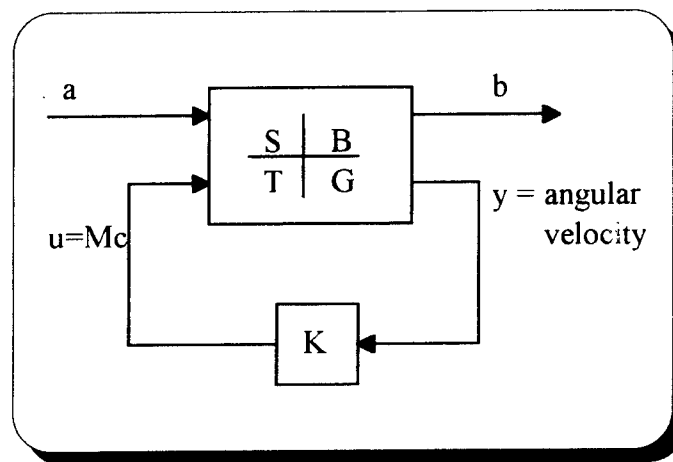


Figure 3. System Block Diagram

The controller inputs are of the form

$$\begin{aligned} u &= Ky \\ \frac{a}{EI}M_c &= K\dot{\theta} \end{aligned} \quad (2.44)$$

Combining compensator  $K$  with the output equation given by (2.42) gives

$$u = KTa + KGu \quad (2.45)$$

or

$$u = HTa \quad (2.46)$$

where

$$H = K(I - GK)^{-1} \quad (2.47)$$

or, in other words,

$$K = H(I + HG)^{-1} \quad (2.48)$$

The closed loop system between  $a$  and  $b$  can be determined by combining equation (2.46) with (2.41)

$$b = Sa + BHTa = (S + BHT)a \quad (2.49)$$

or

$$b = S_{cl}a \quad (2.50)$$

where  $S_{cl}$  is the closed loop scattering matrix.

For the system derived in Section 1, the four block form equation can be determined from the transformation (2.26) and equation (2.40).

$$\begin{Bmatrix} \dot{w} \\ \dot{\theta} \\ \frac{a}{EI}M \\ \frac{a}{EI}Q \end{Bmatrix} = \left(\frac{1}{2}\right) \begin{bmatrix} \sqrt{2}p & 0 & \sqrt{2}p & 0 \\ p^{\frac{2}{3}} & p^{\frac{2}{3}} & -p^{\frac{2}{3}} & p^{\frac{2}{3}} \\ 0 & \sqrt{2}p & 0 & -\sqrt{2}p \\ -p^{\frac{2}{3}} & p^{\frac{2}{3}} & p^{\frac{2}{3}} & p^{\frac{2}{3}} \end{bmatrix} \begin{Bmatrix} a_1 \\ a_2 \\ b_1 \\ b_2 \end{Bmatrix} \quad (2.51)$$



The input equation (2.44) can be determined by using the second and third row equations in (2.51) above.

$$\dot{\theta} = \frac{1}{2}p^{\frac{3}{2}}a_1 + \frac{1}{2}p^{\frac{3}{2}}a_2 - \frac{1}{2}p^{\frac{3}{2}}b_1 + \frac{1}{2}p^{\frac{3}{2}}b_2 \quad (2.52)$$

$$\frac{a}{EI}M_c = \sqrt{2}pa_2 - \sqrt{2}pb_2 \quad (2.53)$$

The above two equations are combined producing

$$\dot{\theta} = p^{\frac{3}{2}}a_1 + p^{\frac{3}{2}}a_2 - \left(\frac{p}{2}\right)^{\frac{1}{2}}M_c \quad (2.54)$$

Equations (2.40) and (2.54) form an equation appropriate for a control system design.

$$\begin{Bmatrix} b_1 \\ b_2 \\ \dot{\theta} \end{Bmatrix} = \begin{bmatrix} -1 & 0 & 0 \\ 0 & 1 & -\sqrt{2}p^{-1} \\ p^{\frac{3}{2}} & p^{\frac{3}{2}} & -\left(\frac{p}{2}\right)^{\frac{1}{2}} \end{bmatrix} \begin{Bmatrix} a_1 \\ a_2 \\ M_c \end{Bmatrix} \quad (2.55)$$

The first row of this equation can be dropped since  $b_1$  cannot be physically controlled by  $M_c$ . This wave mode is called a "far field" mode since it represents a mode transmitted along the beam's axis for a long distance. Therefore, the closed loop system  $S_{cl}$  can be determined.

$$\begin{aligned} S_{cl} &= \begin{bmatrix} 0 & 1 \end{bmatrix} + \left(-\sqrt{2}p^{-1}\right)H \begin{bmatrix} p^{\frac{3}{2}} & p^{\frac{3}{2}} \end{bmatrix} \\ &= \begin{bmatrix} -X & 1 - X \end{bmatrix} \end{aligned} \quad (2.56)$$

where

$$X = \sqrt{2}Hp^{-\frac{1}{2}} \quad (2.57)$$

**b. H infinity Compensator Design**

In order to minimize the effect of the incoming waves on the outgoing waves, it is desirable to choose a compensator  $K$  for which the "magnitude" of the closed loop scattering matrix is minimized. This is motivated by drawing energy out of the system at the junction point where the actuator is located.

The magnitude of a matrix can be measured by its norm. One type of matrix norm is the H infinity norm which is given by

$$\|S_{cl}\|_{\infty} = \sup(\bar{\sigma}[S_{cl}(j\omega)]) \quad (2.58)$$

$\bar{\sigma}$  is the largest singular value. The singular values can be found by

$$\sigma_i(S_{cl}) = \sqrt{\lambda_i(S_{cl}^* S_{cl})} \quad (2.59)$$

where  $S_{cl}^*$  is the complex conjugate of  $S_{cl}$ , and  $\lambda_i$  are the eigenvalues of the matrix in parentheses. The eigenvalues are found by

$$S_{cl}^* S_{cl} = \begin{bmatrix} -X(-j\omega) \\ 1 - X(-j\omega) \end{bmatrix} \begin{bmatrix} -X(j\omega) & 1 - X(j\omega) \end{bmatrix} \quad (2.60)$$

$$\begin{vmatrix} \lambda - X(j\omega)X(-j\omega) & X(-j\omega)[1 - X(j\omega)] \\ X(j\omega)[1 - X(-j\omega)] & \lambda - [1 - X(j\omega)][1 - X(-j\omega)] \end{vmatrix} = 0 \quad (2.61)$$

Solving the determinant above leads to

$$\bar{\sigma}^2 = \lambda = 2 \left[ X(j\omega) - \frac{1}{2} \right] \left[ X(-j\omega) - \frac{1}{2} \right] + \frac{1}{2} \quad (2.62)$$

The smallest solution for equation (2.62) occurs at  $X(s) = \frac{1}{2}$  which gives  $\bar{\sigma} = \frac{1}{\sqrt{2}}$ . Now equation (2.57) can be solved for  $H$ .

$$H = \frac{1}{2\sqrt{2}} \left(\frac{a}{s}\right)^{\frac{1}{2}} \quad (2.63)$$

Using equation (2.48)  $K$  can be determined as

$$K = \frac{2}{3\sqrt{2}} \left(\frac{a}{s}\right)^{\frac{1}{2}} \quad (2.64)$$

As seen in equation (2.44)  $K$  gives the relationship between the angular velocity,  $\dot{\theta}$ , and the actuator moment,  $M_c$ . However, the sensor for the FSS beam gives the angle  $\theta$  for an output. Thus it is desired to find a transfer function from  $\theta$  to  $M_c$ . This transfer function can be found by taking the Laplace transform of (2.44).

$$\frac{a}{EI} M_c(s) = K s \theta(s) \quad (2.65)$$

Combination of this equation with (2.8) and (2.64) yields

$$C(s) = \frac{M_c(s)}{\theta(s)} = \frac{\sqrt{2} (EI)^{\frac{3}{4}} (\rho A)^{\frac{1}{4}}}{3} \sqrt{s} \quad (2.66)$$

This transfer function was derived for a beam clamped at the base and free at the end. The transfer function above was also derived for a pinned-free beam by Matsuda and Fuji [Ref. 3] using the H-infinity approach. A similar transfer function was found by MacMartin and Hall [Ref. 5] by minimizing the H infinity norm of the power flow into the system. MacMartin and Hall also point out that this solution extracts half of the power at all frequencies. This is in contrast to other controllers which are more effective at a given mode, but cannot add significant damping at all of the modes at the same time.

The control law given in (2.66) is effectively a "half differentiator". It is similar to velocity feedback with a forty five instead of a ninety degree phase lead. In order to implement this control law the function  $\sqrt{s}$  must be estimated by a rational

transfer function. As shown by MacMartin and Hall [Ref. 5], this irrational function can be approximated over a wide frequency range by a finite number of zeros and poles spaced logarithmically along the negative real axis. Figure 4 shows the Bode plot for four zeros and four poles.

$$\sqrt{s} = \frac{(s+10^{-4})(s+10^{-2})(s+10^0)(s+10^2)}{(s+10^{-3})(s+10^{-1})(s+10^1)(s+10^3)} \quad (2.67)$$

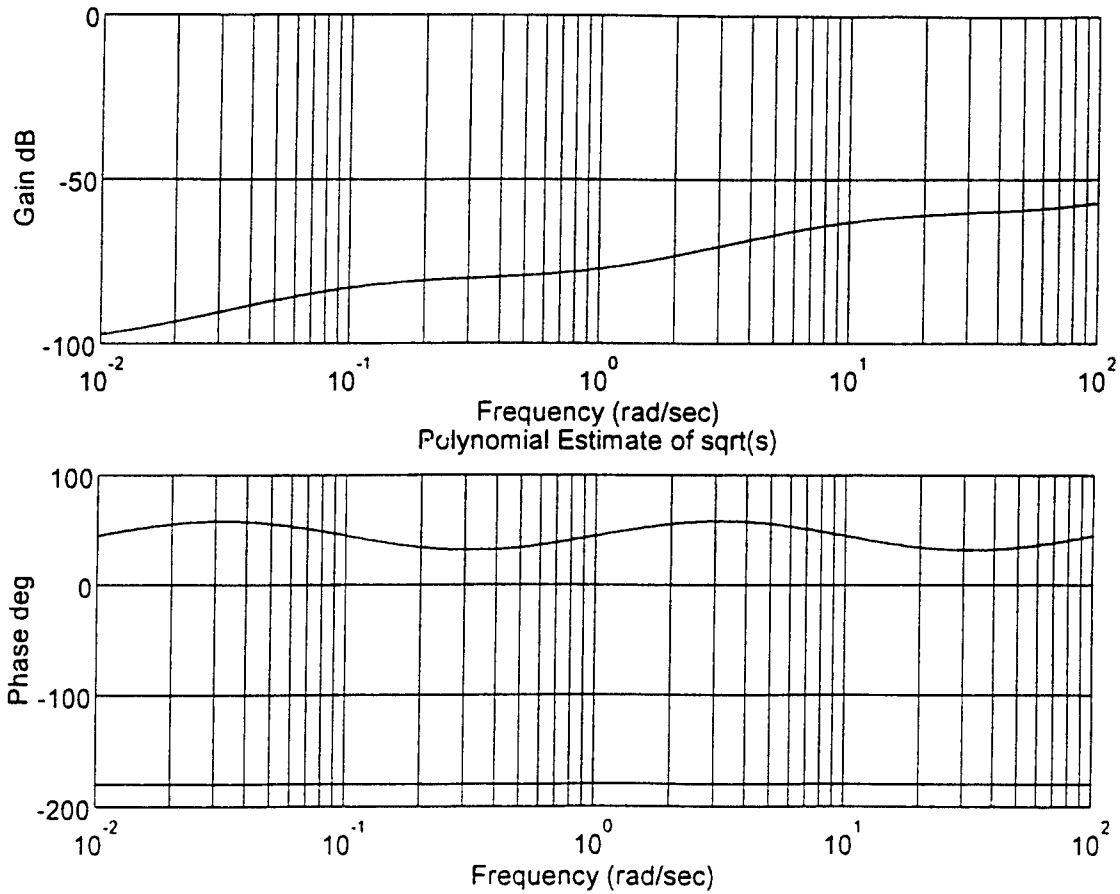


Figure 4. Rational Estimate of  $\sqrt{s}$

## B. SENSOR AND ACTUATOR

The sensors and actuators for the FSS beam are nearly collocated at the base and can be seen in Figure 5. Both the sensor and actuator are made of piezoelectric ceramic. As seen in the figure, the piezoelectric wafers are stacked. This allows for high sensitivity from the sensor and more actuator power in a small area.

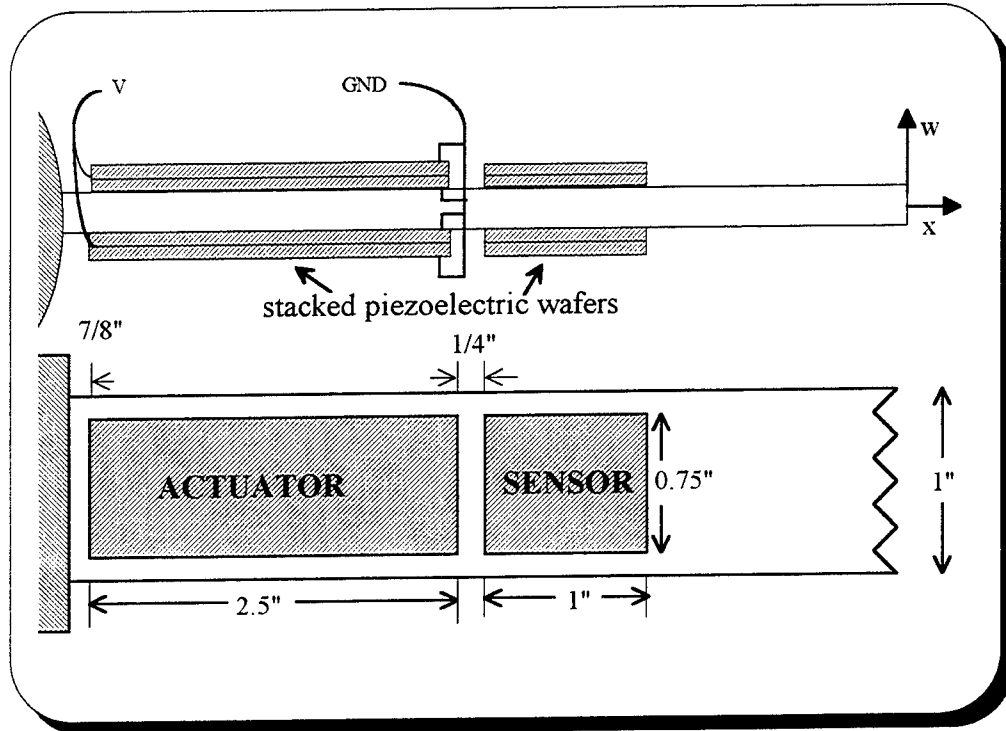


Figure 5. First Beam Element with Sensor Actuator Pair

### 1. Piezoelectric Material

Piezoelectric ceramics have many advantages as actuators and sensors. Table 1 shows the advantages of using piezoelectric materials in structural vibration control.

[ Ref. 8]

The usefulness of piezoelectric ceramics in vibration control is derived from their ability to convert electrical energy into mechanical energy and vice versa. When a force is

applied to the material, it creates a voltage proportional to the applied force. Conversely, when an electric potential is applied across the ceramic, it creates mechanical strain.

Sensor	Actuator
high strain sensitivity	high stiffness
low noise	sufficient stress to control vibrations
low-moderate temperature sensitivity	good linearity
easily implemented	low power consumption
	easily implemented

Table 1. Advantages of Piezoelectric Ceramics

## 2. Sensor

It can be shown that a piezoelectric material produces voltage proportional to strain when force is applied. [Ref. 9] This voltage is given by the equation

$$V_s = t_s \left( \frac{Ed_{31}}{D} \right) (1 - \nu) \epsilon_x \quad (2.68)$$

The material constants for the Navy Type II PZT, which is used in this study, are given in Table 2.

Constant	Description	Units	Value
$d_{31}$	Lateral Strain	m/V or Coul/N	1.8e-10
E	Young's Modulus	Pascal (N/m <sup>2</sup> )	6.30e10
$\nu$	Poissons Ratio	n/a	0.35
D	Abs Permittivity	Farad/m or N/V <sup>2</sup>	1.5e-8
$t_s$	Sensor Thickness	m	2 x 1.905e-4
$t_b$	Beam Thickness	m	1.588e-3
A	Sensor Area	m <sup>2</sup>	4.839e-4

Table 2. Material Constants for Navy Type II PZT

The strain developed at the cross section of the beam at a distance  $h$  from the midplane of the beam is

$$\varepsilon_x = -h \frac{\partial^2 w}{\partial x^2} \quad (2.69)$$

Combine this equation with (2.68) to get

$$V_s(x) = k \frac{\partial^2 w}{\partial x^2} \quad (2.70)$$

where

$$k = -ht_s \frac{Ed_{31}}{D} (1 - \nu) \quad (2.71)$$

Since the sensor is distributed along the beam, however, the measured sensor output is the average voltage over the length,  $L$ , of the wafer.

$$V_a = \frac{k}{L} \int_{x_p}^{x_{p+1}} V_s(x) dx \quad (2.72)$$

$$= \frac{k}{L} \int_{x_p}^{x_{p+1}} \frac{\partial^2 w}{\partial x^2} dx$$

$$= \frac{k}{L} \left[ \frac{\partial w}{\partial x} \right]_{x_p}^{x_{p+1}} = \frac{k}{L} [\theta_{p+1} - \theta_p]$$

$$V_a = \frac{k}{L} \theta \quad (2.73)$$

Thus, the voltage output of the sensor is directly proportional to the effective bending angle over the sensor element. The value of  $\frac{k}{L}$  for the FSS beam is  $-1.378 \times 10^{-4}$  rad/volt.

### 3. Actuator

The actuator produces a moment proportional to the voltage across its terminals. The electric field across the wafer is related to the voltage by

$$\Phi = \frac{V}{t_a} \quad (2.74)$$

A lateral strain is induced by this electric field and is given by

$$\varepsilon = d_{31}\Phi \quad (2.75)$$

Furthermore, the stress in the piezoelectric wafer is

$$\sigma = \frac{F_x}{A_x} = E\varepsilon_x \quad (2.76)$$

where  $A_x$  is the wafer cross section. If  $b$  is the width of the actuator, then equations (2.74) to (2.76) can be combined to find the force along the midplane of the actuator.

$$F_x = bEd_{31}V \quad (2.77)$$

Since there is a piezoelectric stack on each side of the beam, the moment developed by the actuator is

$$M = 2bEd_{31}\left(\frac{t_a+t_b}{2}\right)V \quad (2.78)$$

Using  $b = 1.905$  cm. and values from Table 2 this equation becomes

$$M = (.01675 \frac{Nm}{V})V \quad (2.79)$$

Thus, the actuator produces a moment which is proportional to the voltage applied across its terminals.





### III. STRUCTURAL RESPONSE SIMULATION

The open loop transfer function was determined by a modal model which was generated by truncating a desired number of modes. The open loop transfer function,  $G(s)$ , and the H-infinity controller,  $H(s)$ , were then discretized and formed into the closed loop system as shown in Figure 6.

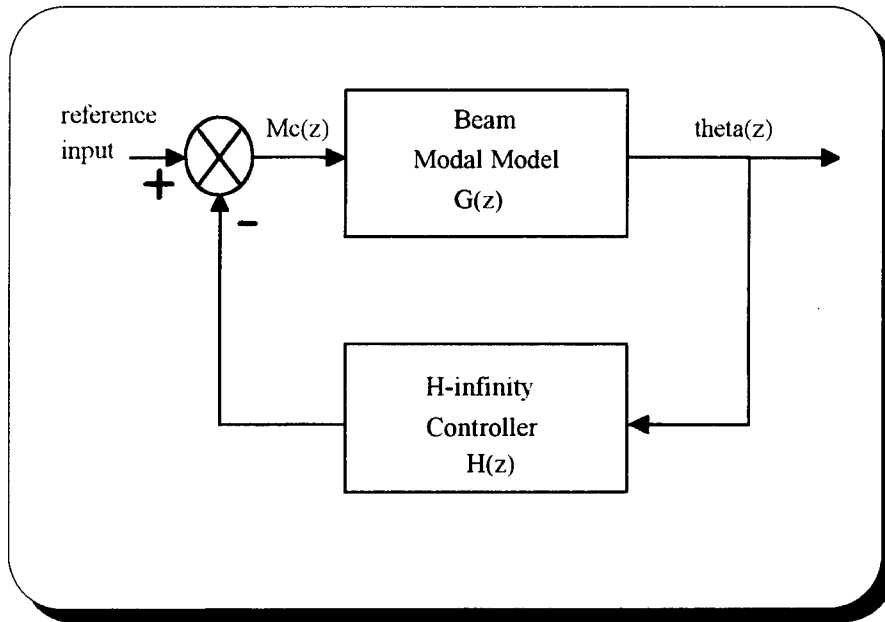


Figure 6. System Block Diagram

#### A. OPEN LOOP TRANSFER FUNCTION

The beam dynamics were determined by a modal model. The equation of motion for a lumped parameter model is given by the matrix equation

$$M\ddot{q} + C\dot{q} + Kq = F(t) \quad (3.1)$$

where

$M$  is the mass matrix

$C$  is the damping matrix

$K$  is the stiffness matrix

$q$  is the vector of generalized coordinates

The beam is modeled with eight finite elements as shown in Figure 7. The mass and stiffness matrices were constructed using the finite element method. [Ref. 10, pp. 300-328] Element mass and stiffness matrices were calculated and combined to form the global mass and stiffness matrices for equation (3.1). These matrices can be seen in the program BEAM.M in the Appendix A. It should be noted that the vertical displacements and rotation at the base are equal to zero due to clamped boundary conditions.

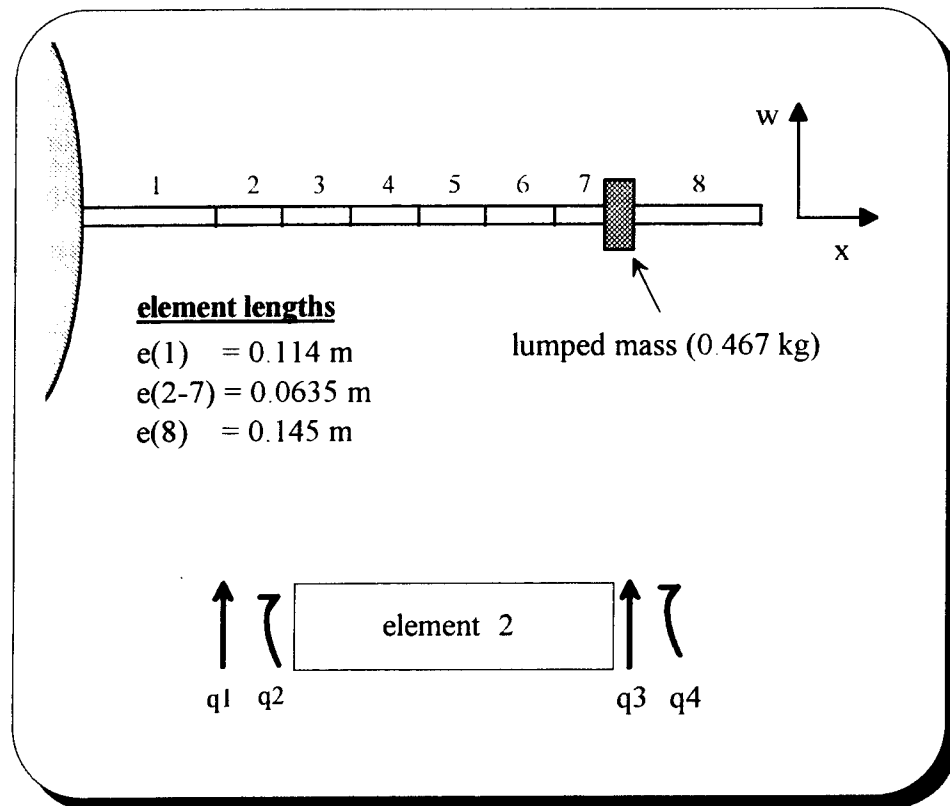


Figure 7. Finite Element Model

The generalized coordinate vector can be decoupled into modal coordinates. [Ref. 11, pp.104-107]

$$q(t) = \begin{Bmatrix} w_1 \\ \theta_1 \\ \bullet \\ \bullet \\ w_8 \\ \theta_8 \end{Bmatrix} = \Phi \eta(t) = \sum_{i=1}^n \phi_i \eta_i(t) \quad (3.2)$$

The vector  $\eta(t)$  contains the modal coordinates, and the modal matrix  $\Phi$  contains the system eigenvectors normalized with respect to the mass matrix. The number of modes,  $n$ , for the lumped parameter model is equal to the number of generalized coordinates. A reasonable solution can be found by truncating the number of modes into a physically meaningful number. For example, three modes are often adequate to describe the longitudinal vibration of a simple cantilevered beam. [Ref. 11, pp. 292-293]

Equation (3.2) is substituted for the generalized coordinates in equation (3.1) and premultiplied by  $\Phi^T$  to get the equation of motion in terms of the modal coordinates.

$$\ddot{\eta} + \Lambda_c \dot{\eta} + \Lambda_k \eta = \bar{F}(t) \quad (3.3)$$

The first coefficient matrix is the modal damping matrix.

$$\Lambda_c = \Phi^T C \Phi = \begin{bmatrix} 2\rho_1 \varpi_1 & 0 & 0 & 0 & 0 \\ 0 & \bullet & 0 & 0 & 0 \\ 0 & 0 & \bullet & 0 & 0 \\ 0 & 0 & 0 & \bullet & 0 \\ 0 & 0 & 0 & 0 & 2\rho_{16} \varpi_{16} \end{bmatrix} \quad (3.4)$$

The modal stiffness matrix is

$$\Lambda_k = \Phi^T K \Phi = \begin{bmatrix} \omega_1^2 & 0 & 0 & 0 & 0 \\ 0 & \omega_2^2 & 0 & 0 & 0 \\ 0 & 0 & \bullet & 0 & 0 \\ 0 & 0 & 0 & \bullet & 0 \\ 0 & 0 & 0 & 0 & \omega_{16}^2 \end{bmatrix} \quad (3.5)$$

and the modal force vector is

$$\bar{F}(t) = \Phi^T F(t) = \Phi^T \left\{ \begin{array}{c} 0 \\ M_c \\ 0 \\ \bullet \\ \bullet \\ \bullet \\ 0 \\ 0 \end{array} \right\} \quad (3.6)$$

Note that since the actuator is mounted on the first element, the external moment,  $M_c$ , is applied to the second coordinate,  $q(2) = \theta_1$ .

The modal matrix equation (3.3) can be separated into its individual equations in the form

$$\ddot{\eta}_i + 2\rho_i \omega_i \dot{\eta}_i + \omega_i^2 \eta_i = \bar{f}_i u(t) \quad i = 1, 2, \dots, n \quad (3.7)$$

The Laplace transform of this equation is

$$s^2 \eta_i + s 2\rho_i \omega_i \eta_i(s) + \omega_i^2 \eta_i(s) = \bar{f}_i U(s) \quad (3.8)$$

which leads to the transfer function for  $\eta_i(s)$  and  $U(s)$  as follows

$$\frac{\eta_i(s)}{U(s)} = \frac{\bar{f}_i}{s^2 + 2\rho\omega_i s + \omega_i^2} \quad (3.9)$$

Equation (3.9) gives the transfer function from the input,  $U(s)$ , to the  $i$ -th modal coordinate,  $\eta_i$ , where  $i = 1, 2, \dots, 16$ .

Now, the system transfer function for a physical coordinate can be determined. The output equation for a single input, multiple output system is

$$y(t) = C_1 q(t) \quad (3.10)$$

As discussed in Chapter II, the piezoelectric sensor mounted on the first element measures the angle  $\theta_1$ . Thus the output equation becomes

$$y(t) = \theta_1(t) = \begin{bmatrix} 0 & 1 & 0 & \bullet & \bullet & 0 \end{bmatrix} q(t) \quad (3.11)$$

$$\theta_1(t) = q_2(t) \quad (3.12)$$

This equation leads to a single input, single output system. Using the transformation to modal coordinates given by equation (3.2), the output equation becomes

$$\theta_1(t) = \sum_{i=1}^n \phi_{2,i} \eta_i(t) \quad (3.13)$$

where  $\phi_{2,i}$  denotes elements of second row of  $\Phi$ . Convert this equation to the  $s$  domain using the Laplace transform. Therefore,

$$\theta_1(s) = \sum_{i=1}^n \phi_{2,i} \eta_i(s) \quad (3.14)$$

Combining this equation with (3.9), and the fact that the input  $U(s) = M_c(s)$ , yields the open loop transfer function.

$$G(s) = \frac{\theta_1(s)}{M_c(s)} = \sum_{i=1}^n \frac{\phi_{2,i}f}{s^2 + 2\rho_i\omega_i s + \omega_i^2} \quad (3.15)$$

As seen in Figure 8, one way to view equation (3.15) is  $n$  single transfer functions combined in parallel. This can be easily implemented using the Matlab™ Control Systems Toolbox "parallel.m" command.

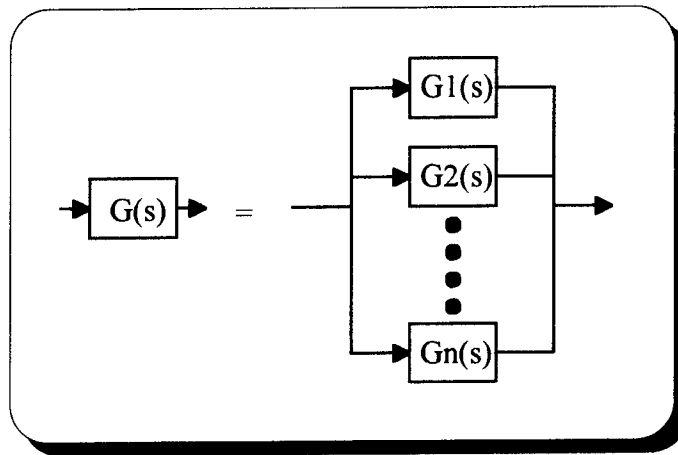


Figure 8. Open Loop Transfer Function

## B. DISCRETE TRANSFER FUNCTIONS

Each transfer function was transformed to the  $z$  (discrete) domain before forming the closed loop system. The relationship between the  $s$  (continuous) and  $z$  (discrete), is

$$z = e^{sT} \quad (3.16)$$

where  $T$  is the sampling period and  $s = -\alpha + j\omega T$ .

The open loop transfer function, determined by equation (3.15) was converted to a discrete transfer function using a Tustin transformation. The Tustin transformation shown below is the Pade approximation to the exponential (3.16). [Ref. 12, pp. 253-282]

$$z = \frac{1 + \frac{sT}{2}}{1 - \frac{sT}{2}} \quad (3.17)$$

The Tustin transformation maintains the frequency response of the continuous system while preserving the mapping of the s-plane into the z-plane.

The transfer function for the estimated H-infinity controller was transformed to the z domain by the matched pole zero technique. Recall from Chapter II that the H-infinity controller was irrational and was estimated using zeros and poles spaced logarithmically along the negative real axis. These zeros and poles can be mapped directly to the z domain by replacing each zero or pole term  $s + a$  with its discrete equivalent,  $z - e^{-aT}$ . The gain for the discrete transfer function is chosen so that  $G(z)|_{z=1} = G(s)|_{s=0}$ . [Ref. 12, pp.304-305] Using Matlab™ the equivalent form of equation (2.64) is

$$G(z) = k \frac{(z+1.000000)(z+.999995)(z+.995012)(z+.606531)}{(z+.999995)(z+.999500)(z+.951229)(z+.006738)} \quad (3.18)$$

### C. CLOSED LOOP SYSTEM

Control of the beam was simulated by closing the loop using H infinity controller, ( $\sqrt{s}$ ) and derivative ( $s$ ). Also, a second order filter was incorporated to study the effects of filtering the sensor output in the system. The closed loop transfer function was determined using the feedback command in Matlab™.

### D. SIMULATION RESULTS

The open and closed loop Bode plots for the H-infinity controller are shown in Figure 9. The plot shows a reduction in magnitude over a broad frequency range as expected.



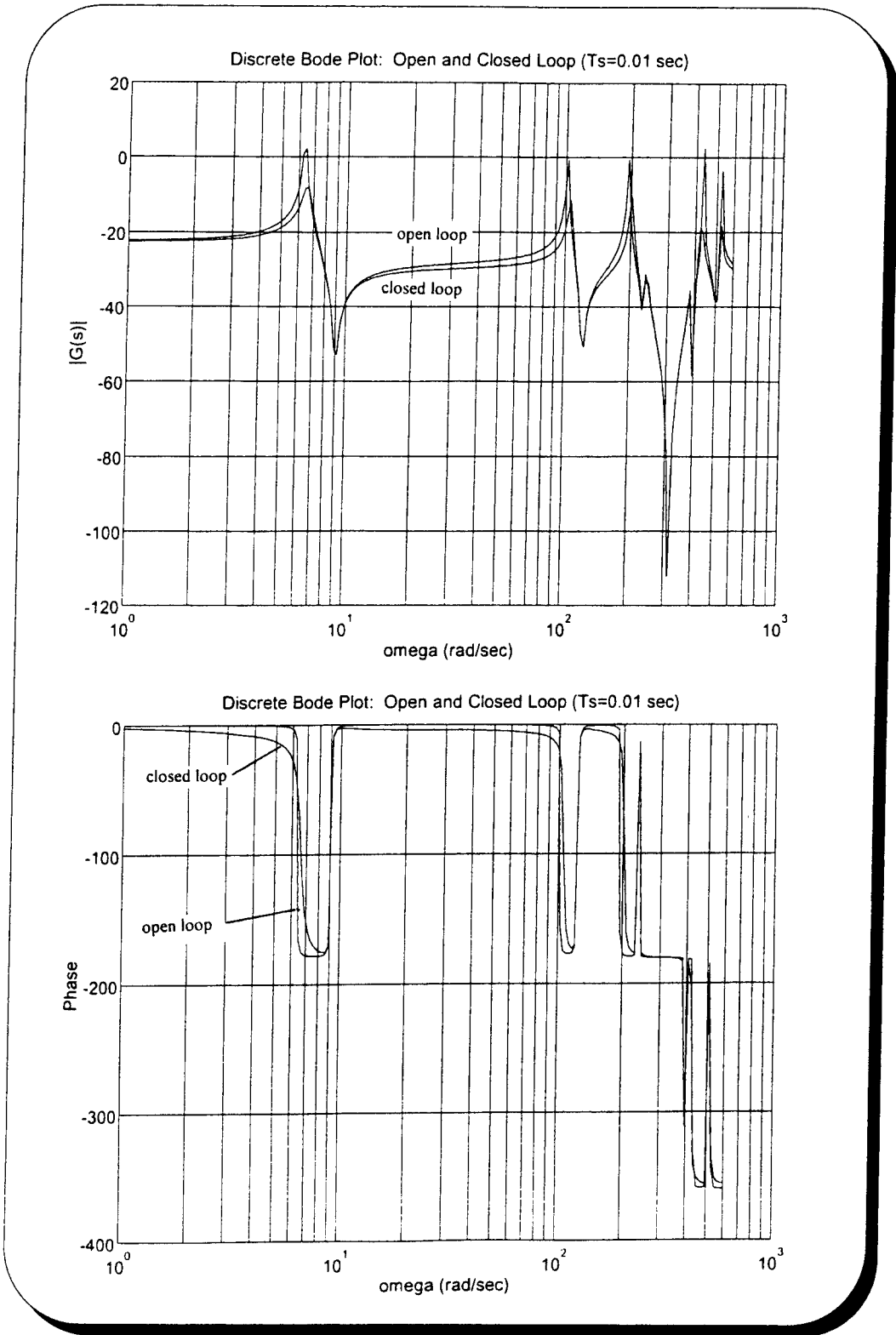


Figure 9. Open and Closed Loop Bode Plots

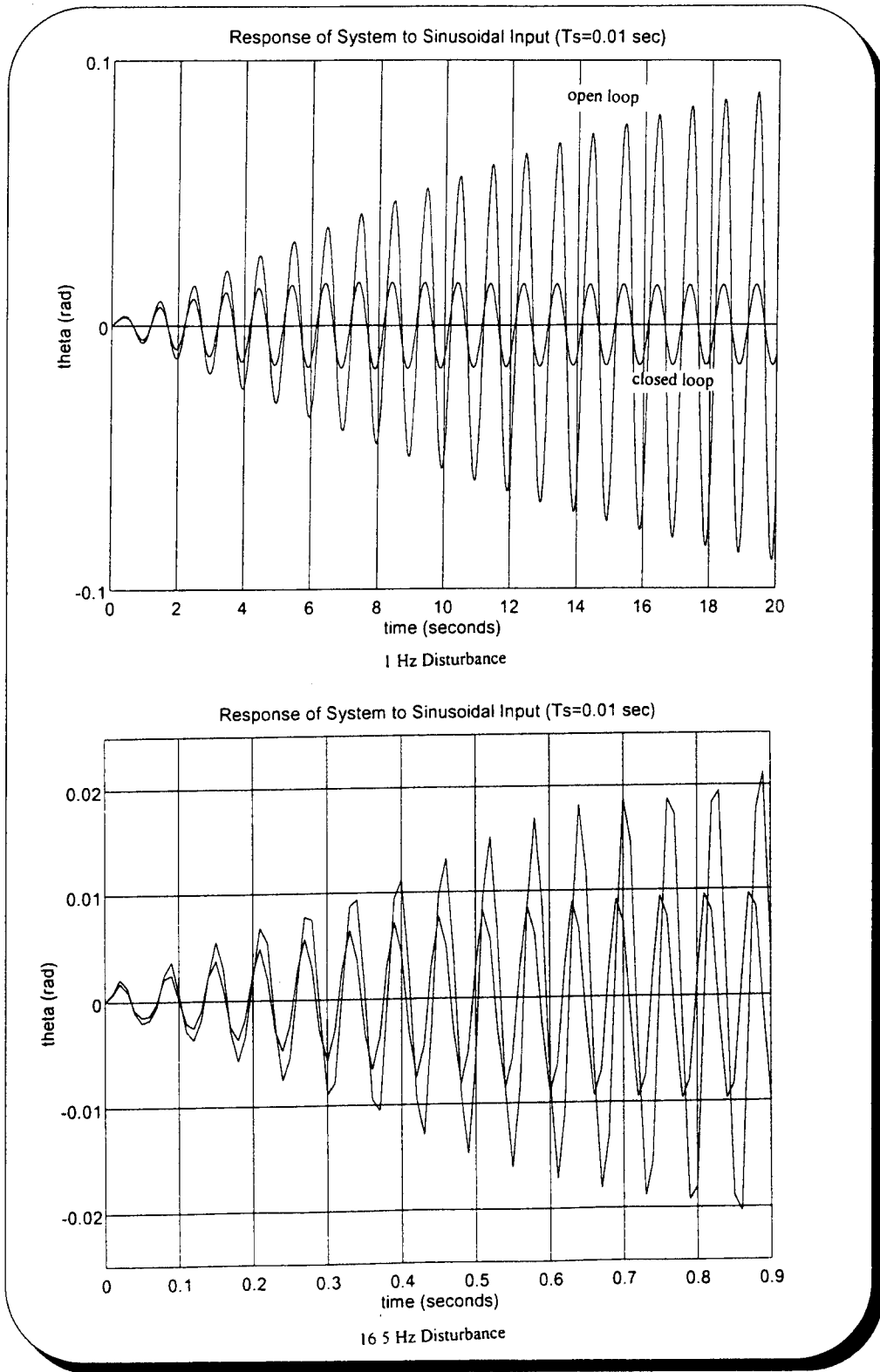


Figure 10. Forced Response

The Bode plot becomes inaccurate at frequencies above the Nyquist rate of 314 radians per second due to the system being discrete with a sampling period of 0.01 seconds.

Figure 10 shows the time response to a sinusoidal input of 1 Hz which is the first natural frequency of the beam. This plot shows a dramatic reduction in the amplitude of the closed loop system for the first two modes (1 and 17 Hz).

## IV. EXPERIMENTAL ANALYSIS

### A. SET UP

The wave absorbing controller was implemented on the Flexible Spacecraft Simulator at the Naval Postgraduate School. Figure 11 shows an overall picture of the system.

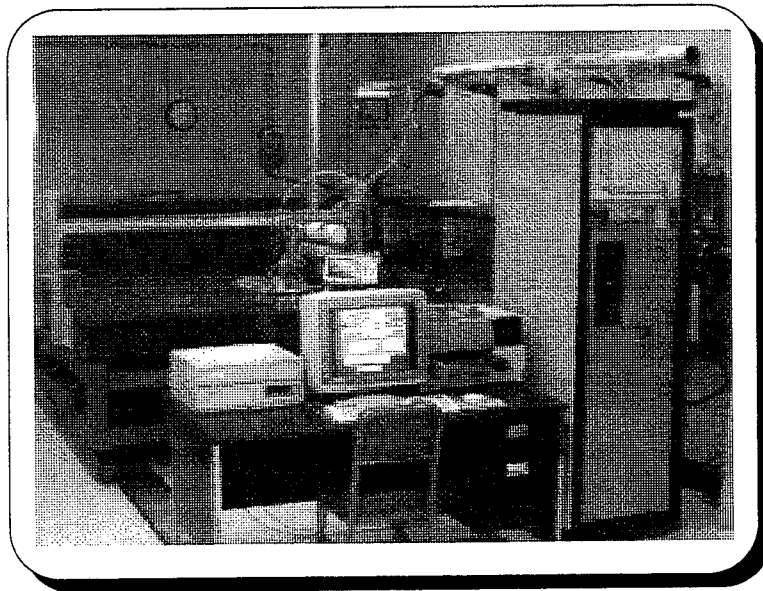


Figure 11. Flexible Spacecraft Simulator

The spacecraft simulator consists of a center body which floats over a granite table on air pads and rotates around an air bearing. A momentum wheel is mounted on the body to allow for slew maneuvers and in this experiment is used as a disturbance source. The flexible beam is attached to the center body as shown in Figure 12.

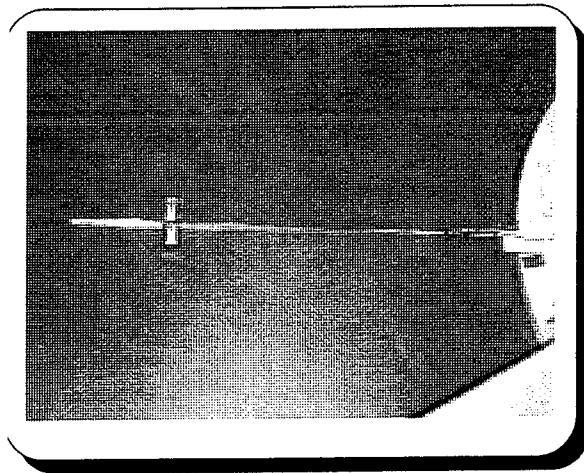


Figure 12. Flexible Beam

The beam is controlled by a piezoelectric sensor-actuator pair mounted at the base of the beam as seen in Figure 13. The dimensions of the sensor and actuator are shown in Figure 5, Chapter II.

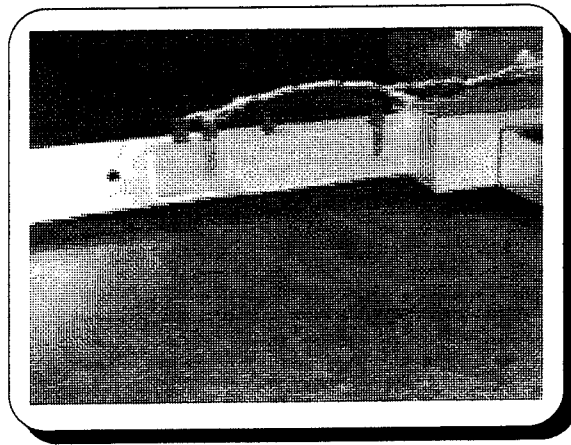


Figure 13. Sensor and Actuator

The digital control system was implemented using Matrix<sub>x</sub><sup>TM</sup>, System Build<sup>TM</sup>, and AC-100<sup>TM</sup> control hardware. The control law was designed using block diagrams in System Build<sup>TM</sup>. The system was then compiled, linked and loaded into the AC-100<sup>TM</sup>, a real time controller. Figure 14 shows the control software block diagram.

Discrete Super-Block    Sampling Interval First Sample    Ext.Inputs    Ext.Outputs    Enable    Parent  
 visi    0.0100    0.    18    9    Parent

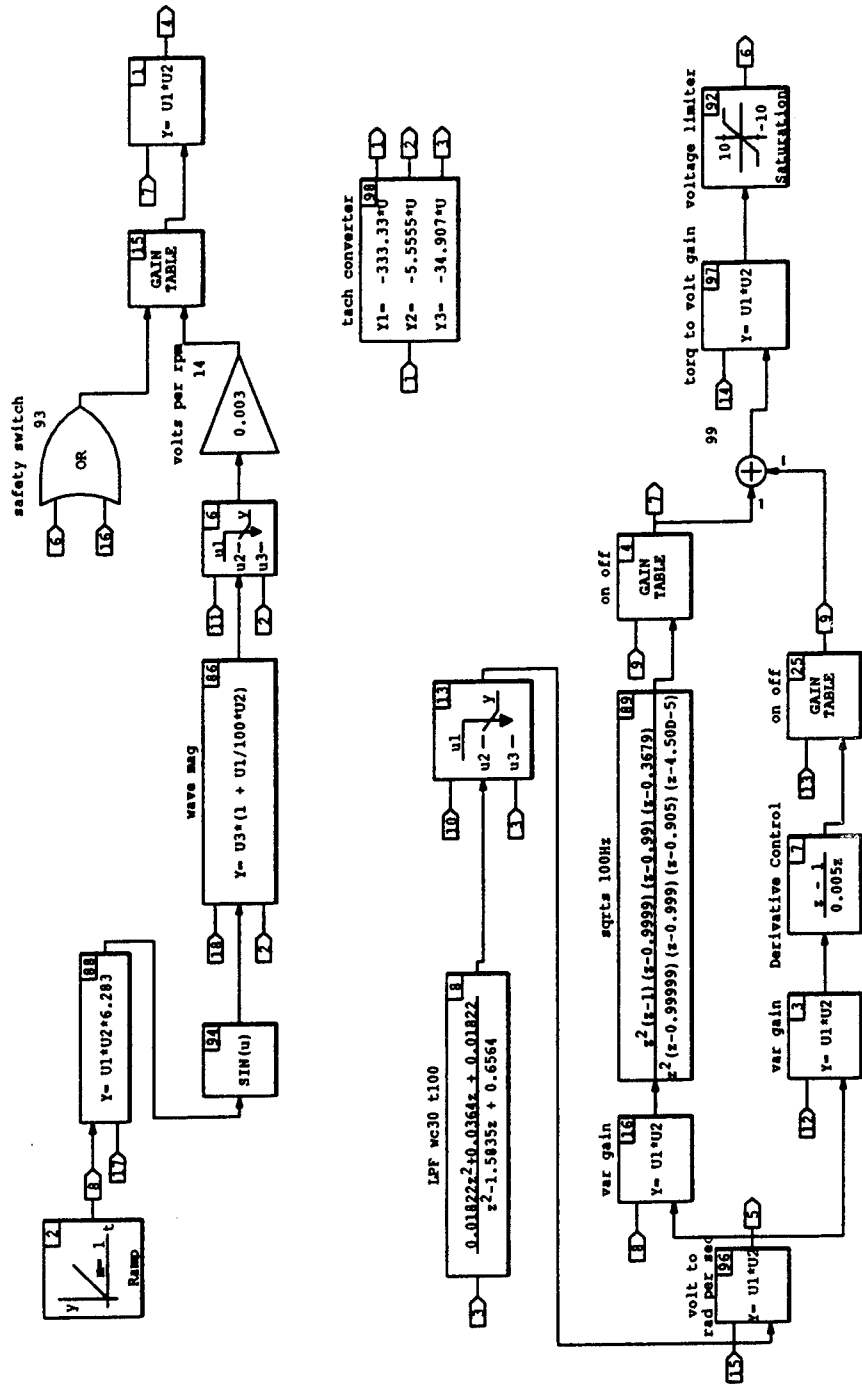


Figure 14. Control System Block Diagram

The AC-100™ has an output of plus or minus 10 Volts. This signal was amplified by two Kepco™ amplifiers connected in series. This allowed a range of plus or minus 75 Volts for the piezoelectric actuator input.

The momentum wheel was used as a disturbance force and is controlled by voltage with 1 Volt per 300 RPM. In order to provide a disturbance torque at a desired frequency the momentum wheel was spun up to a set RPM, then the wheel RPM was modulated at the desired frequency. The control blocks for the momentum wheel are also shown in Figure 14.

## **B. EXPERIMENTAL RESULTS**

### **1. Initial Tests**

The initial choice for the digital sampling rate was 100 Hz. Sampling rates of 50, 200, and 400 Hz. were also used. The 100 and 200 Hz sampling rates appeared to be a reasonable choice.

The main difficulty at the initial stages of the experiment was high frequency noise coming from the sensor. Whenever there was a large jump in the sensor signal between samples, the output to the actuator would have a large jump in voltage, causing the actuator to click. These voltage jumps, possibly as high as 150 Volts, could cause damage to the piezoelectric actuator. Thus, different sampling rates were tried. The higher sampling rates worked well at reducing the voltage steps between samples, since the sampling period was shorter, making the actuator output closer to continuous. However, the higher sampling rates also allowed more of the higher frequency noise into the system. The lower sampling rates, allowed less noise in the system, but had large voltage jumps between samples.

The solution to these problems was to insert a low pass filter at the sensor output. A number of filters of different orders and cutoff frequencies were tried. The final choice was a second order filter with a damping ratio of 0.707 and a cutoff frequency of 30 radians per second (4.8 Hz). This filter, combined with a 100 Hz sampling rate, allowed good, stable performance for H-infinity and derivative control.

## 2. Free Response of the Beam

The free response of the beam was tested for the first two modes. The beam was set to an initial condition and allowed to vibrate freely. The plots for response of the first two modes are shown in Figures 15 and 16. Note that the second mode plot data was collected at a rate of 500 Hz for more accuracy. In order to get a good plot of the second mode the data was filtered using a high pass FIR filter with a cutoff frequency of 14 Hz. This filtered out the dominant first mode and allowed for a better view of the second mode.

The damping ratio of each mode was determined by noting that the amplitude of the wave at any time,  $t$ , is determined by

$$A(t) = A_0 e^{-\zeta \omega_n t} \quad (4.1)$$

where  $A_0$  is the initial amplitude and  $\omega_n$  is the frequency of that mode. If the amplitude is measured at two different points on the plot the damping ratio can be found by solving for  $\zeta$ .

$$\zeta = \frac{\ln\left(\frac{A_0}{A(t)}\right)}{\omega_n t} \quad (4.2)$$

The damping ratios of the first two modes are shown in Table 3.

Mode	Frequency (Hz / (rad/sec) )	Damping Ratio
1	0.95 / 5.97	$3.7 \times 10^{-3}$
2	17.0 / 106.8	$3.9 \times 10^{-3}$

Table 3. Free response damping ratios

The damping ratios determined experimentally were used for the finite element program described in Chapter III. The higher modes were estimated to be about the same for the program. Also, note that the first two natural frequencies agree well with the program frequencies of 1.01 and 17.8 Hz.



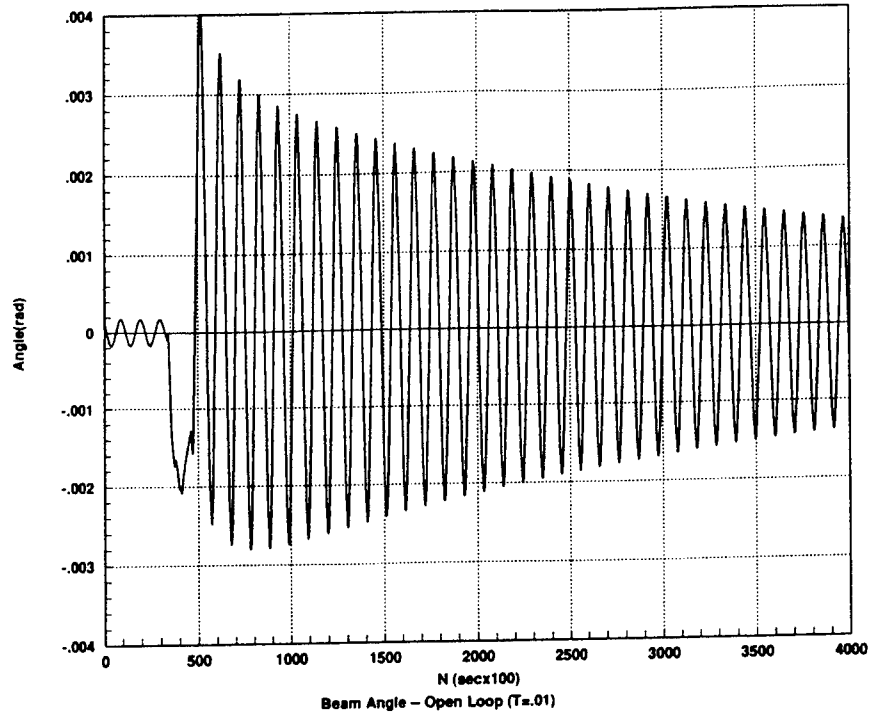


Figure 15. Free Response, Mode 1 (0.95 Hz)

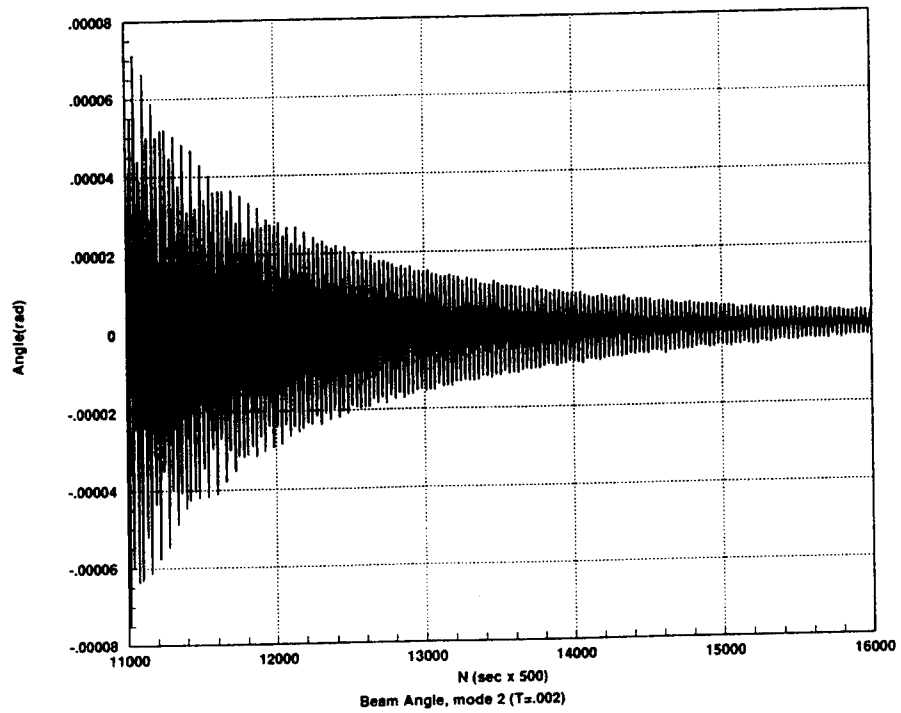


Figure 16. Free Response, Mode 2 (17 Hz)

### 3. Initial Condition Response with Active Control

In this part of the experiment, the response of the beam to an initial condition was tested with two different control laws. The first was the H-infinity (or  $\sqrt{s}$ ) controller, and the second was a derivative control. As pointed out in Chapter II, the H-infinity controller in this case is similar to the derivative control. It provides a phase lead of 45 degrees instead of 90 for the derivative controller. Its magnitude rolls off more sharply compared to the derivative controller at higher frequencies.

The results are shown in Figures 17 and 18. A damping ratio for each case was calculated in a similar fashion to the free response in the previous section. The measured frequencies and calculated damping ratios are shown in Table 4.

	Frequency (Hz)	Damping Ratio
Free Response	0.95	$3.9 \times 10^{-3}$
H-infinity Control	0.98	$3.7 \times 10^{-2}$
Derivative Control	0.96	$3.9 \times 10^{-2}$

Table 4. Damping Ratios

From the results in Table 4 the derivative controller seems to be slightly better than the H-infinity controller at this frequency. However, as can be seen in Figure 18, the derivative controller began to excite the second mode after about 30 seconds. The derivative controller was also much more sensitive to noise in the system and often caused spikes in the voltage signal sent to the actuator. The H-infinity controller, on the other hand, was less sensitive to noise and gave a smoother input to the actuator. The H-infinity controller turns out to produce reliable performance and was more stable.

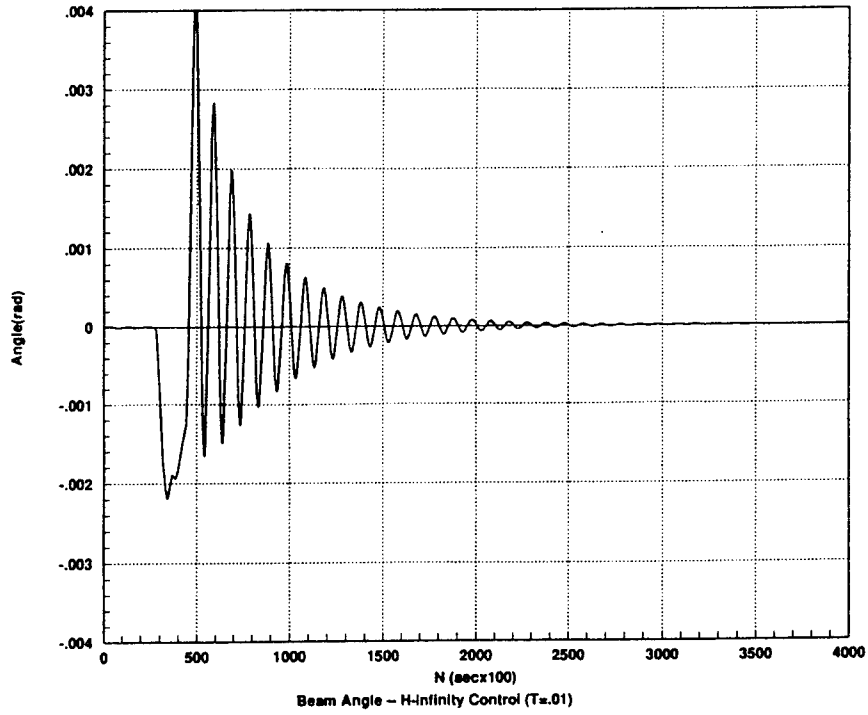


Figure 17. Initial Condition Response using H-infinity Control

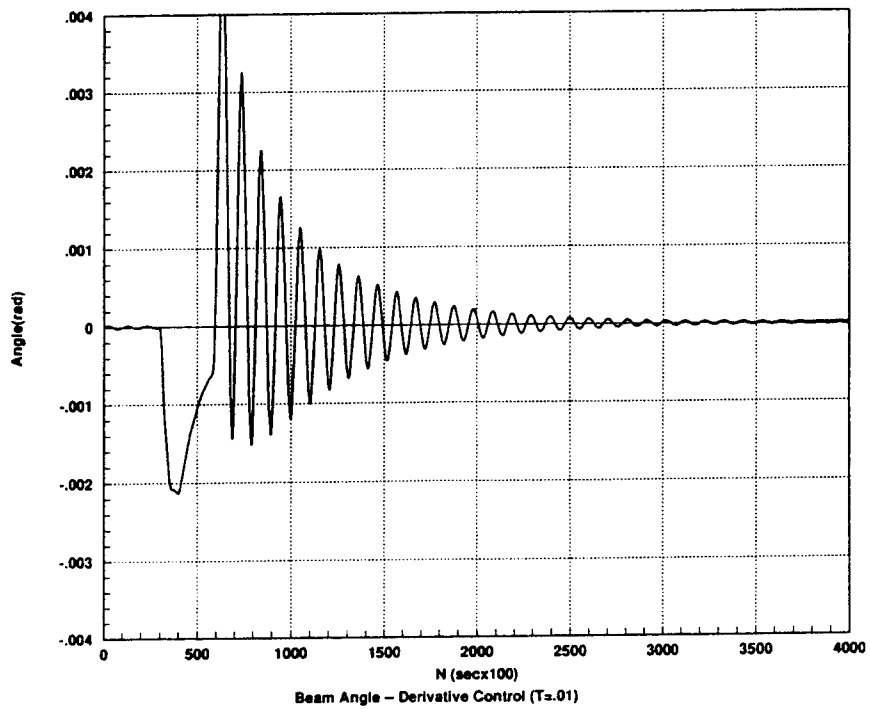


Figure 18. Initial Condition Response using Derivative Control

#### 4. Forced Response

The forced response of the closed loop system was tested using the momentum wheel as a disturbance source. Different runs were made using different frequencies. Both H-infinity and derivative control laws were implemented.

As discussed previously, the system had stability problems with high frequency noise and large voltage jumps. Thus, there was a necessity to use a low pass filter. Initially first and second order filters with 30, 50 and 100 rad/sec cutoff frequencies were used. The most stable performance was achieved using a second order 30 rad/sec filter. This reduced the effective bandwidth of the controller to 4.8 Hz. Also, the filter began to reduce the amount of phase lead of the controller as the disturbance frequency came near 4.8 Hz.

The controller did, however, work well within the low pass bandwidth with significant active control action near the first natural mode of 1 Hz. The results of closing the control loop are given in Figures 19 and 20. The decrease in amplitude for both controllers was calculated and is shown in Table 5.

Controller	(Initial/Final) amplitude	Decrease in amplitude(dB)
H-infinity	5	14
Derivative	3.35	10.5

Table 5. Controller performance (1 Hz disturbance)

The H-infinity controller performed better in this case. A significant reason for this was that the H-infinity controller was less sensitive to noise and, therefore, the gain could be increased to get full use of the 150 V peak to peak output of the actuator amplifier. The derivative controller became unstable if the gain was increased too much, even with the low pass filter. Figure 20 shows that the derivative controller begins to excite higher modes after about 55 seconds. The H-infinity controller, combined with the second order filter, showed no tendency to excite the higher modes when subjected to the disturbance. The H-infinity controller had the best performance with a forced response.

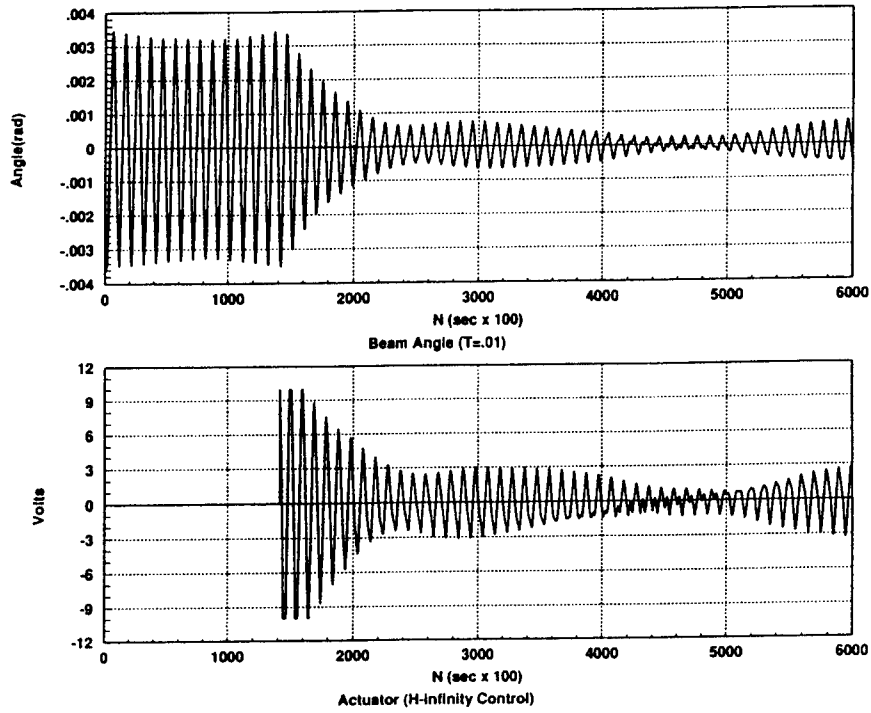


Figure 19. Forced Response, H-infinity Control (1 Hz disturbance)

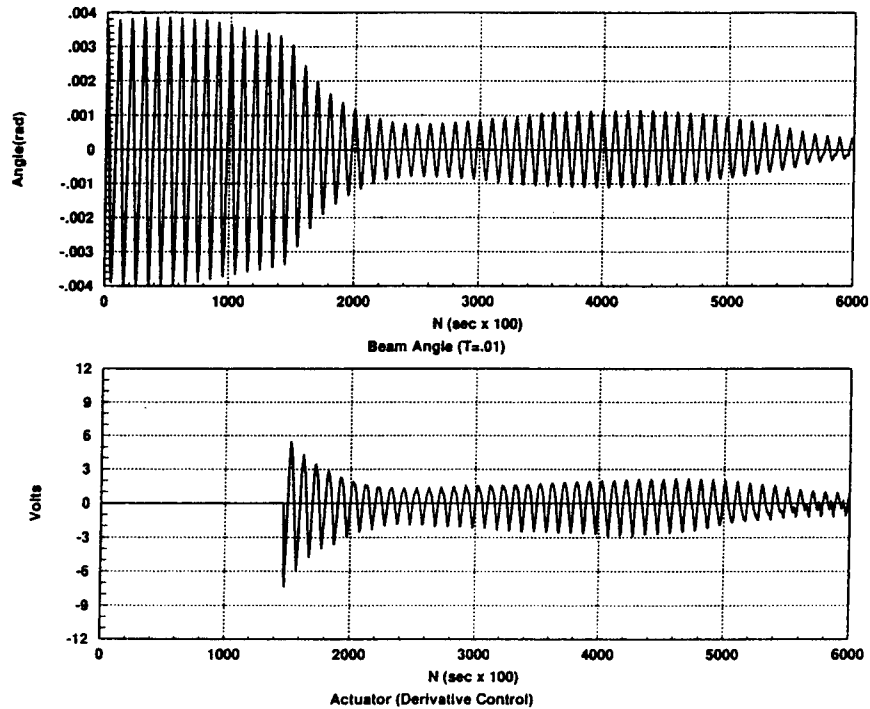


Figure 20. Forced Response, Derivative Control (1 Hz disturbance)

## V. SUMMARY AND CONCLUSIONS

Active control of flexible spacecraft structures has become an important topic. Larger and lighter structures supporting more sensitive equipment have led to the need for active control of spacecraft structures. This thesis studied a wave absorbing approach to this control problem. A closed loop scattering matrix was derived which determines the relationship between incoming waves, outgoing waves, sensor and actuator. The control law was found by minimizing the magnitude of this closed loop scattering matrix. Theoretically, this approach allows for a relatively simple control law, broadband control, and does not require a modal model of the system for operation.

This control law was then applied to the Flexible Spacecraft Simulator (FSS). The sensing and actuation for the flexible beam was implemented by piezoelectric ceramic wafers mounted at the base of the beam. The control law was tested by simulation on a computer, and then by applying it to the hardware in the lab.

The computer simulation showed that the controller was useful over a broad range of frequencies below the Nyquist rate of the digital system. The results from the FSS confirmed this for frequencies below 5 Hz. At higher frequencies the controller had some problems due to sensor noise requiring a low pass filter, and thus limiting the bandwidth of the system. At the first natural frequency of 1 Hz the H-infinity controller performed well and increased the damping ratio of the system from  $3.93 \times 10^{-3}$  to  $3.7 \times 10^{-2}$ . The controller also decreased the amplitude due to a 1 Hz sinusoidal disturbance by 14 dB.

Some recommendations for further study include adding a weighting function to the terms in the closed loop scattering matrix. This would allow for weighting the output of the controller at desired frequencies. It also allows for implementation of a low pass filter before the H-infinity norm of the matrix is minimized. Another area of study would be the use of analog filters on either the sensor output or the actuator input. The former could be used to filter out noise from the sensor. The latter would be useful in smoothing out the signal sent from the power amplifiers to the piezoelectric actuators. The filters,

however, will change the phase of the closed loop system, which is another area to be addressed. Lastly, the sensor and actuator were assumed to be collocated for this study. Their centers are 1.96 inches apart. This should not be a problem for the lower modes of the system. However, it is possible that at higher frequencies, the phase difference between the wave at the sensor and actuator could cause a stability problem. This could be alleviated by solving the scattering matrix for a noncollocated sensor and actuator.

In conclusion, the use of a wave absorbing controller with piezoelectric sensors and actuators could be a viable approach to vibration suppression of space structures. As discussed by von Flotow [Ref. 13] and Fuji, Ohtsuka and Murayama [Ref. 6], eventually, this approach can be applied to large flexible spacecraft structures with multiple noncollocated sensors and actuators. The wave absorbing control approach combined with new sensor and actuator technology such as piezoelectric ceramics presents a wide area for further research.

```

%*****
%                               Beam Simulator                               *
%
%   This program models a beam 27 inches long with lumped masses*
%   to change the natural vibration frequencies. The beam is      *
%   modeled using a finite element model with 8 elements. The     *
%   transfer function (theta/moment at element 1) of the beam is  *
%   found using modal truncation. The program allows a variety of *
%   control laws to be tested by the user. Included are the H     *
%   infinity controller (sqrt(s)), Derivative, and Integral       *
%   control. Also a second order filter with a variable cutoff    *
%   frequency can be applied to the H infinity or Derivative      *
%   controller.                                                    *
%
%*****
clear

m=.112014;      % linear mass density (kg/m)
ml=.4672;       % lumped mass (kg)
I1=2.0436e-4;   % lumped mass rotary moment of inertia (kgm^2)
h=.0635;        % elemental length (m)
h1=.1143;       % 1st element length (m)
h8=.14478;      % 8th element length (m)
I=8.46825e-12; % beam cross sectional moment of inertia (kgm^2)
E=71e9;         % Youngs modulus (aluminum)
n=8;            % # of elements
dampf=0.0036;   % Estimated damping ratio for beam (Exp from 1st 2
modes)
f=zeros(2*n,1); % force vector (actuator)
f(2)=1;
kh=0.182926;    % H infinity gain (due to beam properties)
T=0.01;         % Sampling period for discretized system

% Elemental mass and stiffness

m11=m*h*[156 22*h;22*h 4*h^2]/420;
m22=m*h*[156 -22*h;-22*h 4*h^2]/420;
m12=m*h*[54 -13*h;13*h -3*h^2]/420;
m21=m12';

m11e8=m*h8*[156 22*h8;22*h8 4*h8^2]/420;
m22e8=m*h8*[156 -22*h8;-22*h8 4*h8^2]/420;
m12e8=m*h8*[54 -13*h8;13*h8 -3*h8^2]/420;
m21e8=m12e8';

% Global mass matrix

gm(1:2,1:2)=m22+m11;
gm(1:2,3:4)=m12;

```



```

for i=1:n-2
    gm(2*i+1:2*i+2,2*i-1:2*i)=m21;
    gm(2*i+1:2*i+2,2*i+1:2*i+2)=m22+m11;
    gm(2*i+1:2*i+2,2*i+3:2*i+4)=m12;
end

gm(2*n-1:2*n,2*n-3:2*n-2)=m21;
gm(2*n-1:2*n,2*n-1:2*n)=m22;

gm(13:14,13:14)=m22+m11e8;
gm(15:16,13:14)=m21e8;
gm(13:14,15:16)=m12e8;
gm(15:16,15:16)=m22e8;

% Add lumped mass (possible 9 nodes)
MI=[m1 0; 0 I1];
node=8;
p=2*(node-1);
gm(p-1:p,p-1:p)=gm(p-1:p,p-1:p)+MI;

% Elemental stiffness matrices

k11=E*I*[12 6*h;6*h 4*h^2]/h^3;
k22=E*I*[12 -6*h;-6*h 4*h^2]/h^3;
k12=E*I*[-12 6*h;-6*h 2*h^2]/h^3;
k21=k12';

k11e8=E*I*[12 6*h8;6*h8 4*h8^2]/h8^3;
k22e8=E*I*[12 -6*h8;-6*h8 4*h8^2]/h8^3;
k12e8=E*I*[-12 6*h8;-6*h8 2*h8^2]/h8^3;
k21e8=k12e8';

% global stiffness matrix

gk(1:2,1:2)=k22+k11;
gk(1:2,3:4)=k12;

for i=1:n-2
    gk(2*i+1:2*i+2,2*i-1:2*i)=k21;
    gk(2*i+1:2*i+2,2*i+1:2*i+2)=k22+k11;
    gk(2*i+1:2*i+2,2*i+3:2*i+4)=k12;
end

gk(2*n-1:2*n,2*n-3:2*n-2)=k21;
gk(2*n-1:2*n,2*n-1:2*n)=k22;

gk(13:14,13:14)=k22+k11e8;
gk(15:16,13:14)=k21e8;
gk(13:14,15:16)=k12e8;
gk(15:16,15:16)=k22e8;

```

```

% Find mode shapes and natural frequencies

[V,D]=eig(gk,gm);
[lambda,k]=sort(diag(D));
V=V(:,k);

factor=diag(V'*gm*V);
phi=V*inv(sqrt(diag(factor)));
omega=diag(sqrt(phi'*gk*phi));
freq=omega/2/pi;
modf=phi'*f;

% Calculate the open loop transfer function of the beam at
% each frequency for the first md modes (truncate).

md=input('Number of modes (1<#<8): ');
s2=diag(ones(md));
s1=2*dampf*omega(1:md);
s0=omega(1:md).*omega(1:md);

num=phi(2,1:md)'.*modf(1:md); % sensor measures theta # 2
den=[s2 s1 s0];
[numg,deng]=parallel(num(1),den(1,1:3),num(2),den(2,1:3));
for i=3:md
    [numg,deng]=parallel(numg,deng,num(i),den(i,1:3));
end

% Discretize open loop system
[numgd,dengd]=c2dm(numg,deng,T,'tustin');

% Control Transfer Function

flag1='y';
while flag1=='y'

    disp('(1) Integral')
    disp('(2) Derivative & Filter')
    disp('(3) sqrt(s)')
    disp('(4) sqrt(s) & Filter: ');
    case=input('Enter Controller Type: ');
    gain=input('Enter gain factor: ');

    %Estimate square root of s
    zrs = [-.0001 -.01 -1 -100];
    pls = [-.001 -.1 -10 -1000];
    nums=poly(zrs);
    dens=poly(pls);

```

```

[numsd,densd]=c2dm(nums,dens,T,'matched');

% Noise filter
wc=input('Enter Filter cutoff frequency (rad/sec): ');
dmpf=.707;
numf=wc^2;
denf=[1 2*dmpf*wc wc^2];
[numfd,denfd]=c2dm(numf,denf,T,'tustin');

if case == 1
    % Integral control
    numhd=gain*[T 0];
    denhd=[1 -1];
elseif case == 2
    % Derivative
    numhd=conv(numfd,[1 -1]);
    denhd=conv(denfd,[T 0]);
elseif case == 3
    numhd=gain*numsd;
    denhd=densd;
elseif case >= 4
    [numhd,denhd]=series(numfd,denfd,gain*numsd,densd);
end

% Closed loop system
[numcld,dencld]=feedback(numgd,dengd,numhd,denhd,-1);

% Frequency Domain Evalutaion.
% Plot Bode for open and closed loop systems.

w=logspace(0,log10(600),200);
[mg,pg]=dbode(numgd,dengd,T,w);
[mc,pc]=dbode(numcld,dencld,T,w);

figure(1)
semilogx(w,20*log10(mg),w,20*log10(mc))
grid
title('Discrete Bode Plot: Open and Closed Loop (Ts=0.01 sec)')
xlabel('omega (rad/sec)')
ylabel('|G(s)|')

figure(2)
semilogx(w,pg,w,pc)
grid
title('Discrete Bode Plot: Open and Closed Loop (Ts=0.01 sec)')
xlabel('omega (rad/sec)')
ylabel('Phase')

% Time Domain Evaluation

```

```

% Plot output of open and closed loop system.

flag='y';
while flag=='y'

    dist=input('Enter disturbance frequency (Hz): ');
    tmax=20/dist;
    nt=0:T:tmax;
    u=0.05*sin(dist.*6.28*nt);
    [yg,xg]=dlsim(numgd,dengd,u);
    [ycl,xcl]=dlsim(numcld,dencld,u);

    figure(3)
    plot(nt,yg,nt,ycl)
    grid
    title('Response of System to Sinusoidal Input (Ts=0.01 sec)');
    xlabel('time (seconds)');
    ylabel('theta (rad)');

    flag=input('Try another disturbance frequency?(y/n) ','s');
end

flag1=input('Try another control law / filter?(y/n) ','s');
end

```



## APPENDIX B

### Finite Element Model

#### Natural Frequencies

1.0e+003 \*

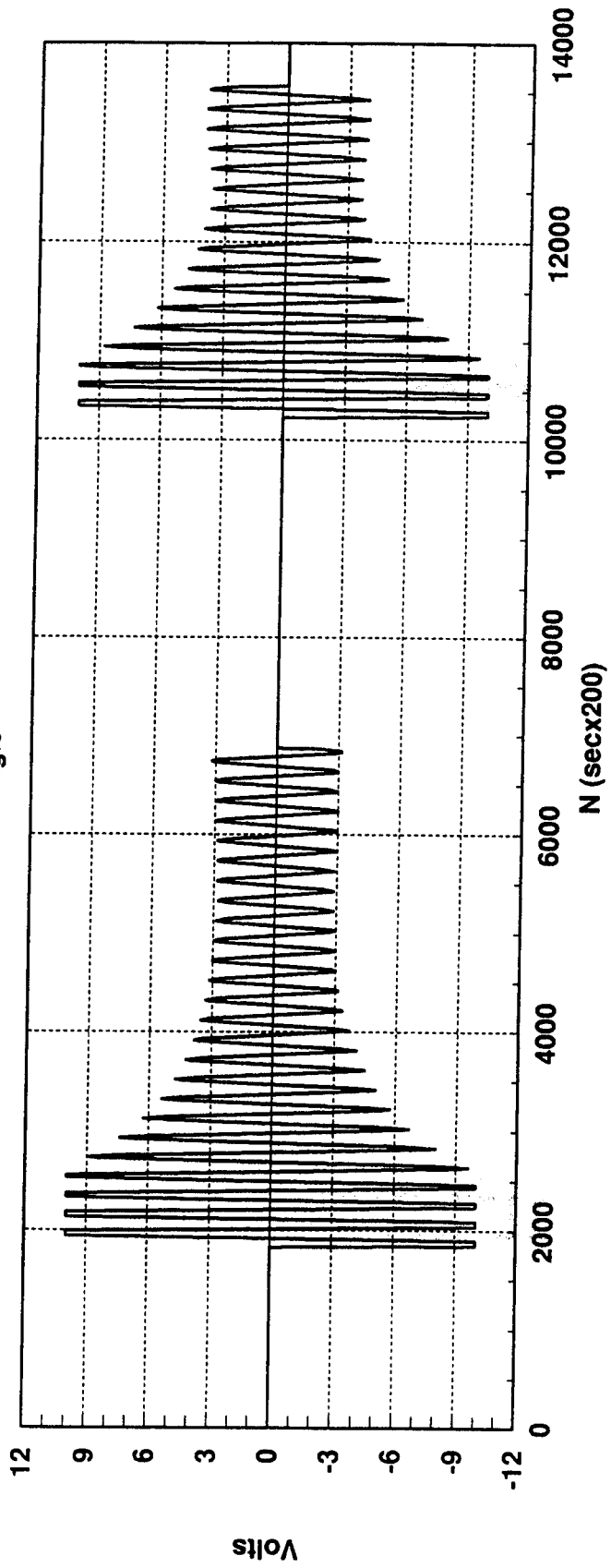
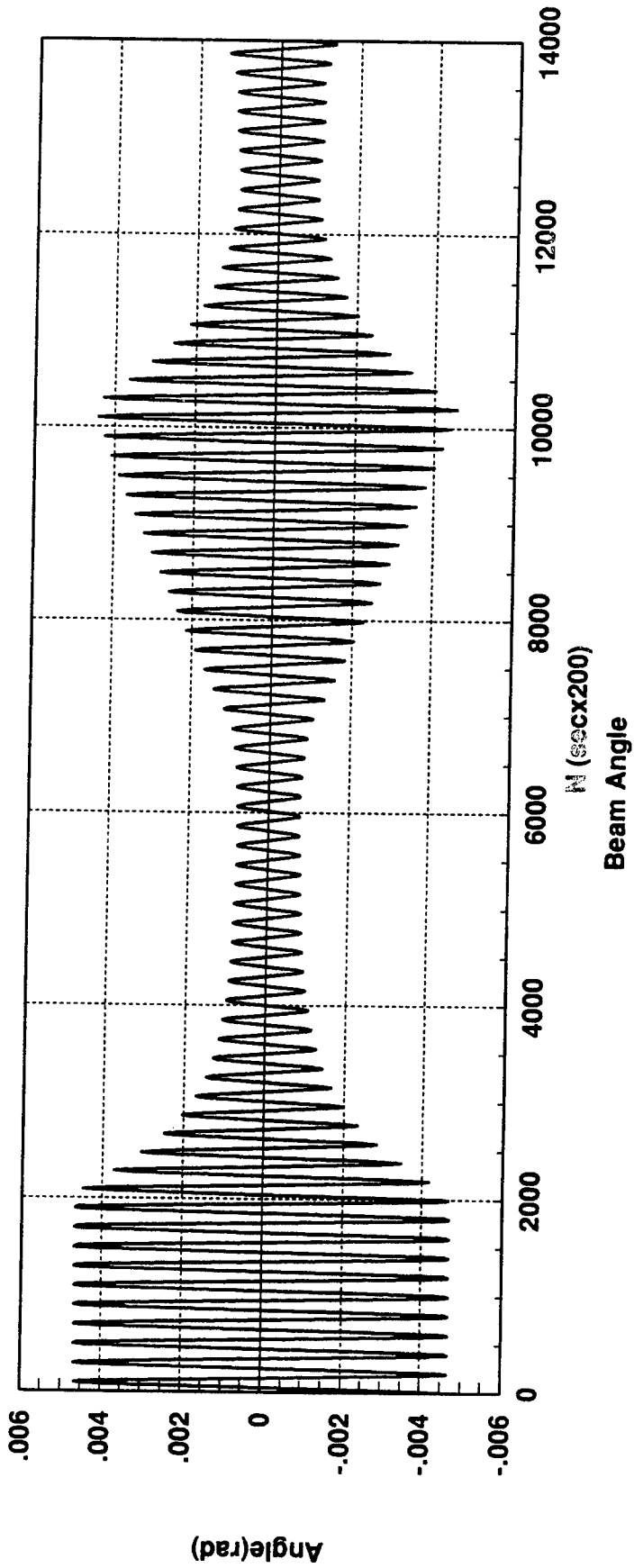
0.00101324976094  
0.01775301423174  
0.04638342775662  
0.07923661265561  
0.11935988578432  
0.22849778748830  
0.37813429140721  
0.56949274733975  
0.61770877977266  
0.79596117358377  
1.16976439767046  
1.54850209877084  
2.04634262642825  
2.68166333705337  
3.45392614581641  
4.22726231062265

»

1.0e+003 \*  
Columns 1 through 7

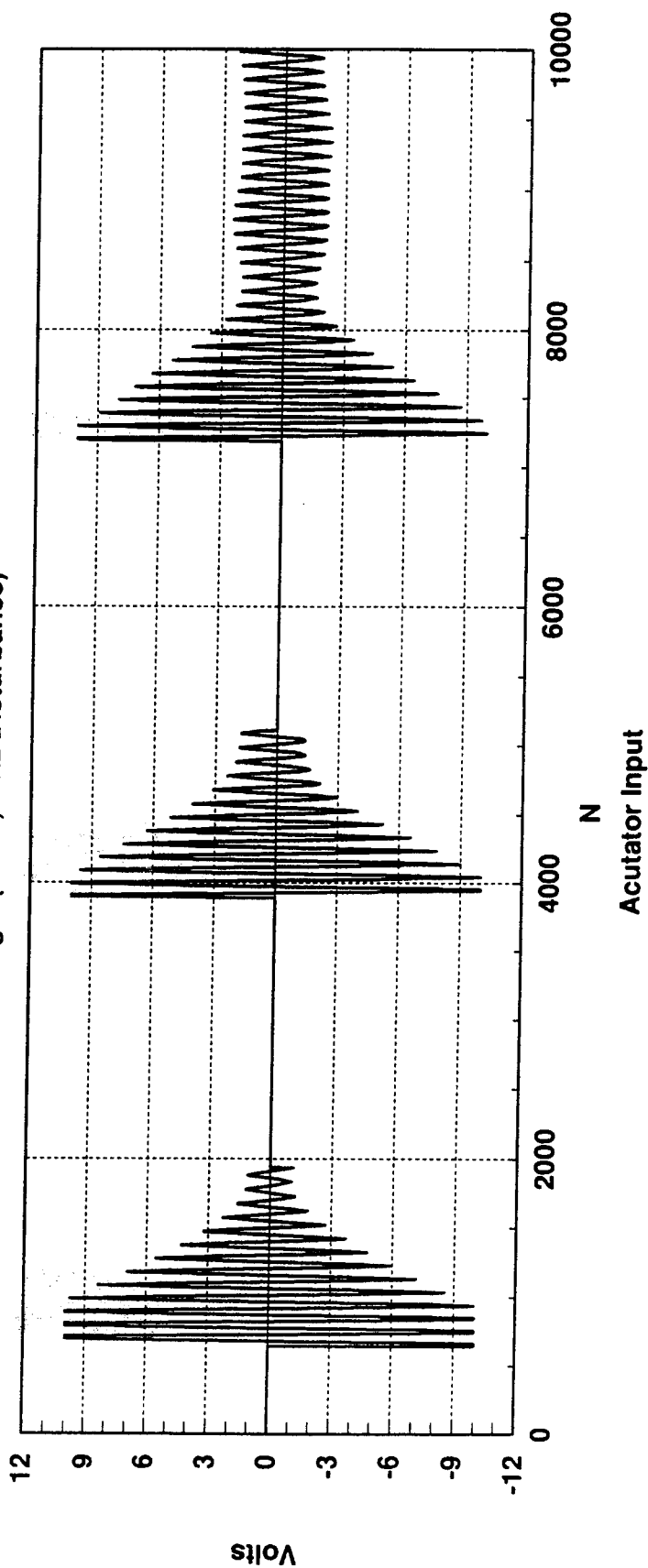
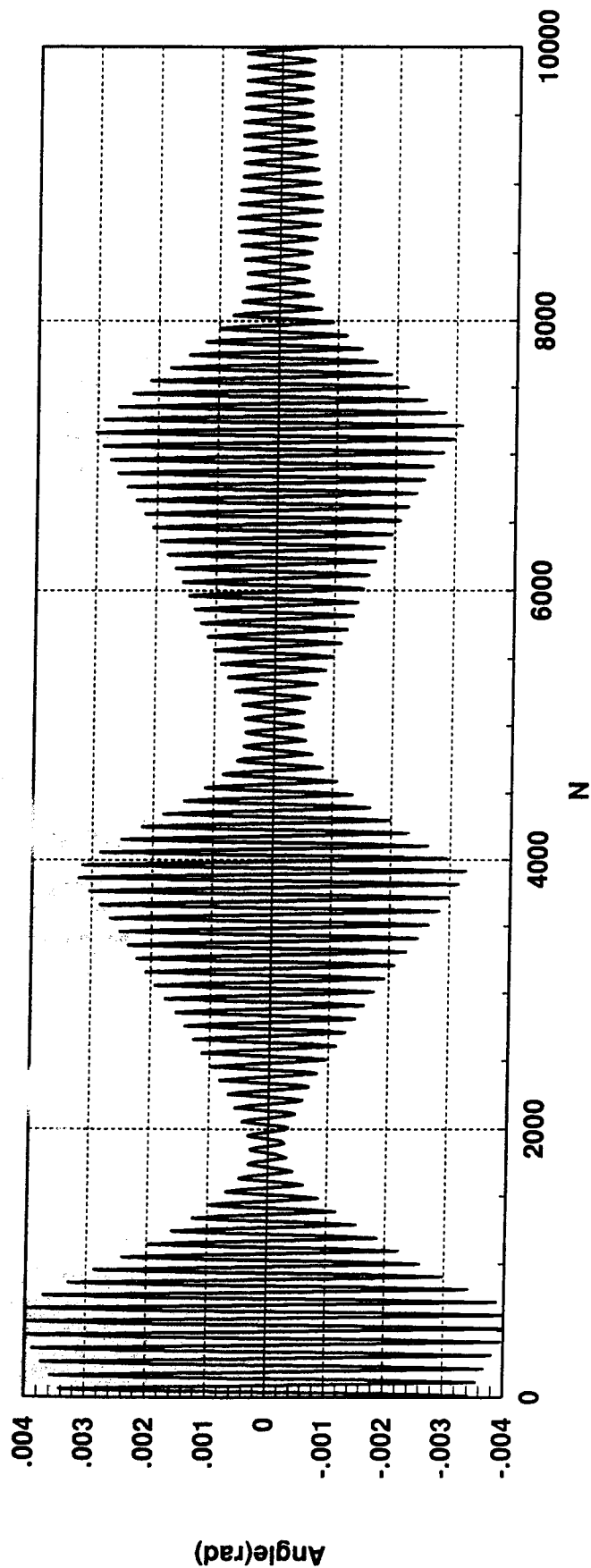
0.0000	0.0005	0.0015	0.0008	0.0035	0.0054	0.0067	0.0070	0.0001	-0.0058	0.0038	-0.0018	-0.0007	0.0027	-0.0036	0.0027
0.0013	0.0142	0.0412	0.0208	0.0782	0.0878	0.0479	-0.0452	-0.0011	0.1629	-0.3549	0.5559	-0.7169	0.8024	-0.7484	0.4795
0.0002	0.0016	0.0043	0.0020	0.0065	0.0046	-0.0007	-0.0056	-0.0001	0.0063	-0.0023	-0.0028	0.0060	-0.0048	0.0005	0.0019
0.0023	0.0195	0.0411	0.0108	-0.0003	-0.1177	-0.2064	-0.1344	-0.0015	-0.0945	0.4203	-0.5095	0.1693	0.5259	-1.1435	1.0360
0.0003	0.0028	0.0061	0.0019	0.0030	-0.0045	-0.0054	0.0022	0.0001	-0.0067	0.0008	0.0058	-0.0035	-0.0039	0.0043	0.0007
0.0032	0.0165	0.0118	-0.0131	-0.1000	-0.1100	0.1106	0.2379	0.0033	0.0333	-0.4591	0.2047	0.5899	-0.6777	-0.5395	1.3528
0.0006	0.0036	0.0057	0.0005	-0.0038	-0.0043	0.0055	0.0021	0.0000	0.0067	0.0008	-0.0058	-0.0035	0.0039	0.0043	-0.0007
0.0039	0.0066	-0.0255	-0.0279	-0.0919	0.1153	0.1064	-0.2392	-0.0042	0.0306	0.4587	0.2072	-0.5885	-0.6791	0.5380	1.3530
0.0008	0.0035	0.0032	-0.0011	-0.0065	0.0048	0.0005	-0.0055	-0.0001	-0.0063	-0.0023	0.0028	0.0060	0.0048	0.0005	-0.0019
0.0044	-0.0085	-0.0469	-0.0193	0.0141	0.1126	-0.2069	0.1376	0.0037	-0.0920	-0.4191	-0.5107	-0.1717	0.5242	1.1433	1.0367
0.0011	0.0024	0.0004	-0.0015	-0.0028	0.0053	-0.0067	0.0070	0.0001	0.0058	0.0038	0.0019	-0.0006	-0.0027	-0.0036	-0.0027
0.0046	-0.0266	-0.0343	0.0093	0.0800	-0.0923	0.0524	0.0415	-0.0013	0.1607	0.3530	0.5551	0.7171	0.8034	0.7497	0.4805
0.0014	0.0001	-0.0002	0.0001	0.0001	-0.0001	0.0001	-0.0001	0.0001	0.0000	0.0000	0.0000	0.0000	0.0000	0.0000	0.0000
0.0048	-0.0458	0.0197	0.0422	-0.0198	0.0084	-0.0049	0.0031	0.0079	0.0022	0.0015	0.0013	0.0011	0.0008	0.0006	0.0003
0.0021	-0.0072	0.0062	-0.0126	0.0016	-0.0003	0.0001	-0.0004	0.0221	0.0001	0.0000	0.0000	0.0000	0.0000	0.0000	0.0000
0.0048	-0.0520	0.0540	-0.1382	0.0223	-0.0063	0.0054	-0.0186	1.1674	0.0037	0.0009	0.0005	0.0003	0.0001	0.0001	0.0000

Mode Shapes



H-infinity control using 200 Hz sampling rate





H-infinity control using 400 Hz sampling rate

## LIST OF REFERENCES

1. Newman, S., *Active Damping Control Of A Flexible Space Structure Using Piezoelectric Sensors And Actuators*, Master's Thesis, Naval Postgraduate School, Monterey, California, 1992.
2. von Flotow, A.H., "Traveling Wave Control for Large Spacecraft Structures", *Journal of Guidance*, Vol. 9, No 4, July August 1986, pp. 462-468.
3. Matsuda, K. and Fuji, H., "H-infinity Optimized Wave-Absorbing Control: Analytical and Experimental Results", *Journal of Guidance, Control and Dynamics*, Vol. 16, No 6, November-December 1993, pp. 1146-1153.
4. von Flotow, A.H., and Shafer, B., "Wave-Absorbing Controllers for a Flexible Beam", *Journal of Guidance*, Vol. 9, No 6, November-December 1986, pp. 673-680.
5. MacMartin, D.G., and Hall, S.R., "Control of Uncertain Structures Using an H-infinity Power Flow Approach", *Journal of Guidance*, Vol. 14, No 3, May-June 1991, pp. 521-530.
6. Fuji, H., Ohtsuka, T., and Murayama, T., "Wave Absorbing Control for Flexible Structures with Noncollocated Sensors and Actuators", *Journal of Guidance, Control and Dynamics*, Vol. 15, No 2, March-April 1992, pp. 431-439.
7. Ogata K., *State Space Analysis of Control Systems*, Prentice-Hall, 1967.
8. Betros, R.S., and Bronowicki, A.J., "Seminar Notes", *Active Damping Workshop*, Spring 1991.
9. Feuerstein, M.G., *A Comparison of Different Control Methods for Vibration Suppression of Flexible Structures using Piezoelectric Actuators*, Master's Thesis, Naval Postgraduate School, Monterey, California, 1994.
10. Meirovitch, L., *Elements of Vibration Analysis*, McGraw-Hill, 1986.
11. Inman, D.J., *Vibration, with Control, Measurement, and Stability*, Prentice-Hall, Inc., 1989.
12. Shahian, B. and Hassul, M., *Control System Design Using Matlab<sup>R</sup>*, Prentice-Hall, 1993.

13. von Flotow, A.H., "Disturbance Propagation in Structural Networks", *Journal of Sound and Vibration*, **106**(3), 1986, pp. 433-450.

## INITIAL DISTRIBUTION LIST

	Number of Copies
1. Defense Technical Information Center Cameron Station Alexandria, Virginia 22304-6145	2
2. Library, Code 052 Naval Postgraduate School Monterey, California 93943-5002	2
3. Chairman, Code AA Department of Aeronautics and Astronautics Naval Postgraduate School Monterey, California 93943-5002	1
4. Chairman, Code SP Department of Aeronautics and Astronautics Naval Postgraduate School Monterey, California 93943-5002	1
5. Commander, Naval Space Command Attn: N112 5280 4th Street Dahlgren, Virginia 22448-5300	1
6. Professor Brij N. Agrawal, Code AA/Ag Department of Aeronautics and Astronautics Naval Postgraduate School Monterey, California 93943-5002	2
7. Professor Hyochoong Bang, Code AA/Ba Department of Aeronautics and Astronautics Naval Postgraduate School Monterey, California 93943-5002	1
8. Lt. Ronald E. Strong, USNR 11040 28th Dr. #331 Phoenix, Arizona, 85029	1